

Forschungszentrum Karlsruhe
Technik und Umwelt

Wissenschaftliche Berichte
FZKA 6482

3-D Monte Carlo Calculations of Energy Deposition of Electrons into Bulk Graphite and into an Inhomogeneous Carbon Plasma Shield

G. Miloshevsky, H. Würz

**Institut für Hochleistungsimpuls- und
Mikrowellentechnik
Projekt Kernfusion**

August 2000

Forschungszentrum Karlsruhe

Technik und Umwelt

Wissenschaftliche Berichte

FZKA 6482

**3-D Monte Carlo Calculations of Energy
Deposition of Electrons into Bulk Graphite and into an
Inhomogeneous Carbon Plasma Shield**

G. Miloshevsky¹, H. Würz

Institut für Hochleistungsimpuls- und Mikrowellentechnik

Projekt Kernfusion

¹permanent address: Luikov Heat and Mass Transfer Institute,
Minsk, 220072 Belarus

This work was performed in the frame of the Belorussian German
WTZ Cooperation Agreement RUS 99/566

Forschungszentrum Karlsruhe GmbH, Karlsruhe
2000

Als Manuskript gedruckt
Für diesen Bericht behalten wir uns alle Rechte vor
Forschungszentrum Karlsruhe GmbH
Postfach 3640, 76021 Karlsruhe
Mitglied der Hermann von Helmholtz-Gemeinschaft
Deutscher Forschungszentren (HGF)
ISSN 0947-8620

3-D Monte Carlo Calculations on Energy Deposition of Electrons into Bulk Graphite and into an Inhomogeneous Carbon Plasma Shield

Abstract

A 3-D Monte Carlo model of the transport of magnetized electrons through a plasma of arbitrary density and temperature gradients is presented. The physical model is based on the division of all the electron collisions into two groups: close and distant. The close collisions with the plasma nuclei and electrons are treated as individual ones. The distant collisions are statistically grouped on some "free path" steps and are described on the base of multiple-scattering theories. The developed models were applied to the calculation of the energy deposition of magnetized mono-energetic and Maxwellian distributed plasma electrons into the inhomogeneous carbon plasma and into bulk graphite shielded by this plasma. The numerical simulation is performed using the 3-D Monte Carlo simulation code MONPLAS.

3-D Monte Carlo Berechnung der Energiedeposition von Elektronen in Graphit und im inhomogenen Kohlenstoffplasma.

Zusammenfassung

Ein 3-D Monte Carlo Modell zur Berechnung des Transports magnetisierter Elektronen durch ein inhomogenes Plasma mit Dichte und Temperaturgradient wird vorgestellt. Elektronenstöße werden als lokal und entfernt behandelt. Lokale Stöße sind individuelle Stöße mit den Plasmaionen und den Elektronen, die entfernten Stöße werden nach der Theorie der Vielfachstreuung behandelt. Die Modelle werden zur Berechnung der Energiedeposition magnetisierter Elektronen in Graphit verwendet. Zur numerischen Simulation wird das 3-D Monte Carlo Programm MONPLAS verwendet. Berechnet werden die Energiedeposition magnetisierter Elektronen im inhomogenen Plasma und in Graphit mit einem inhomogenen Plasmaschild.

Content

1.	INTRODUCTION	1
2.	PHYSICAL MODEL AND INTERACTION PROCESSES	2
2.1	ELECTRON NUCLEAR SCATTERING	4
2.2	ELECTRON-ELECTRON COLLISIONS	6
3.	MONTE CARLO TECHNIQUE	10
3.1	TARGET	10
3.2	SAMPLING PARAMETERS OF INCIDENT ELECTRONS	12
3.3	MACROSCOPIC CROSS SECTIONS	15
3.4	ELECTRON TRANSPORT ALGORITHM	16
3.5	SAMPLING ELECTRON INTERACTIONS	18
3.6	EVALUATION OF THE DISTRIBUTION OF ENERGY DEPOSITION	19
3.7	ACCURACY OF THE MONTE CARLO CALCULATIONS	20
4.	NUMERICAL RESULTS	22
4.1	ENERGY DEPOSITION INTO SOLID TARGETS	22
4.2	ENERGY DEPOSITION INTO A HOMOGENEOUS CARBON PLASMA	23
4.3	ENERGY DEPOSITION INTO GRAPHITE SHIELDED BY A CARBON PLASMA LAYER	26
5.	CONCLUSIONS	28
6.	REFERENCES	30

1. Introduction

The problems associated with the penetration of electrons into plasma have attracted much attention in recent years. It is known that such elements of a tokamak as the divertor is hit by charged particles driven along the magnetic field lines and is exposed to the bombardment by plasma electrons and ions. The power density of the hot plasma incident on the divertor under off-normal conditions can reach 5-10 MW/cm² and its energy is about 10 keV [1]. The action of the magnetized plasma flux on the divertor surface results in heating, melting, evaporation, transition into the plasma state and expansion. Theoretical models describing the behavior of this inhomogeneous medium are based on the magnetohydrodynamic equations with account of radiative transfer [2]. The contribution of the electron fraction of the incident plasma flux to divertor erosion is significantly greater than that of the plasma ions. This is due to the penetration depth of electrons, which is some orders greater than the depth of the plasma ions. Thus, the electrons heat the divertor volumetrically whereas the ions are absorbed in a thin surface layer. The fraction of the electron energy deposited into the divertor depends strongly on the properties of the screening plasma before the divertor. To simulate the erosion rate of the divertor, it is necessary to know the distribution of the energy deposition versus the depth of an inhomogeneous plasma layer and the fraction of energy deposited into the bulk divertor. Thus, it is necessary to have an energy deposition model being capable of predicting the electron range and energy deposition profile as a function of material composition, density, temperature, magnetic field intensity, and the degree of plasma ionization for a variety of incident flux energies.

This report describes a 3-D Monte Carlo approach for investigating the transport of magnetized hot plasma electrons through a plasma layer with density, temperature and magnetic field gradients, and presents some simulation results. This approach involves calculation of scattering data from theoretical scattering cross sections using multiple scattering theories. The calculations of the transport of magnetized electrons in the plasma are performed as a set of computer-generated trajectories. By tracing a large number of such trajectories, it becomes possible to make statistical predictions on the energy deposition.

The plasma electrons have initial energies in the range from 1 keV to 100 keV. Atomic density varies from 10^{15} cm^{-3} up to 10^{19} cm^{-3} . The range of plasma temperature is varied from 0.5 eV up to 250 eV. The energy of the incident electrons is Maxwellian distributed. Density, temperature and magnetic field profiles are given in an arbitrary form. The rotating electrons have different longitudinal and transverse energy components at motion in the plasma. Magnetic field direction with the plasma surface is changed from 0 up to 90 degrees.

In Sec. 2, the physical model and the electron interaction processes are discussed. In Sec. 3, the Monte Carlo technique is presented. Sec. 4 presents the results of Monte Carlo calculations on the energy deposition of the magnetized electrons into solid graphite and into homogeneous and inhomogeneous carbon plasma.

2. PHYSICAL MODEL AND INTERACTION PROCESSES

In the following, the basic assumptions made in the physical model and the processes of multiple scattering and energy loss for the interaction of magnetized electrons with targets are described. Several approximations are made in the physical model of electron transport in the plasma:

- The electrons are moving in the target and interact with scattering centers (plasma electrons and nuclei) which are placed randomly.
- The traversing electrons interact simultaneously with one scattering center.
- The incident electrons do not interact among each other.

Using these assumptions and introducing the notation of the electron trajectory the spatial localization of the interaction can be considered. The electron trajectory is represented as spiral line. When an interaction takes place in inflection points. In the state (direction and energy) of the incident electron and of the plasma particle changes.

Difficulties with electron transport arise from the fact that the cross sections for all the processes (scattering and energy loss) become infinite as the transferred energy approaches zero. In reality, these cross sections, when various corrections are taken into account (i.e., screening for nuclear scattering, electron binding for electron scattering), are not infinite, but they are very large and the exact values for the total cross sections are not well known. The transport of electrons is dominated by the long-range Coulomb force, resulting in large numbers of small interactions. For example, an electron in aluminum slowing down from 500 keV to 62.5 keV will undergo about 10^5 individual interactions. Therefore, a single-collision Monte Carlo approach to electron transport is infeasible for many situations of practical interest. On the other hand, the low momentum transfer events which give rise to the large cross section values do not result in large fluctuations in the behavior of energy deposition. For this reason, they are lumped together and treated in a continuous manner. Cutoff angles and energies are used to distinguish between continuous and discrete interactions. Any electron interaction that produces a delta-electron is considered to be a discrete event. All other interactions are considered continuous and give rise to continuous energy losses and direction changes to the electron between discrete interactions. The energy losses are due to soft interactions with the atomic electrons (excitation and ionization loss). The changes in direction are mostly due to multiple Coulomb scattering from the nucleus, with some contribution coming from soft electron scattering.

Analytic and semi-analytic multiple-scattering theories [3-11] are used to describe these continuous interactions by accounting for them in a cumulative sense including the affect of many such interactions at the same time. These theories attempt to use the fundamental cross sections and the statistical nature of the transport process to predict probability distributions for significant quantities, such as energy loss and angular deflection. Unfortunately, multiple-scattering theories rely on a variety of approximations that restrict their applicability, so that they cannot solve the entire transport problem. In order to follow an electron through a significant energy loss, it is necessary to break the electron's path into many steps. The length of these "free path" steps between discrete interactions is sampled randomly using the total macroscopic cross section, which determines the probability of discrete interactions. The energy loss and angular deflection of the electron during each of the

"free path" steps are sampled from probability distributions based on the appropriate multiple-scattering theories. Along each of these steps, the electron is assumed to follow a spiral line, and the multiple scattering is accounted for by changing the electron's direction at the end of the step. The azimuthal angle is selected randomly. These "free path" steps are sampled to be long enough to encompass many collisions (so that angular multiple-scattering theories are valid) but short enough that the mean energy loss in any one step is small (so that continuous energy loss approximations are satisfied). These steps must also be kept small enough so that neglecting the lateral deflection of the electron along a step does not introduce significant errors, i.e. the true electron path length is not much larger than the spiral line path length. Otherwise, a systematic error in the distance to the next discrete interaction will result.

2.1 Electron nuclear scattering

When an electron passes through a target, it undergoes a large number of elastic collisions with the atomic nuclei. These have the effect of changing the electron's direction, but do not significantly change its energy. A simple Rutherford cross section of the differential form [12]

$$\frac{d\sigma_{en}}{d\Omega} = \left(\frac{Ze^2}{2m_e v^2} \right)^2 \frac{1}{\sin^4 \theta/2} \quad (1)$$

is used to represent the elastic scattering. Here $d\sigma_{en}/d\Omega$ is the differential cross section per unit solid angle, Z the atomic number of the absorbing plasma, e the electronic charge, m_e and v the mass and velocity of the incident electron, θ the angle of deflection. The cross section for elastic scattering from the nucleus is proportional to Z^2 .

The long-range Coulomb interaction of the electrons with the target nuclei causes a high scattering probability at small angles. In our model, the first approximation of the Molière distribution [6,7] is used, i.e. the Gauss function which

takes the scattering at small angles into account. Other terms of the Molière distribution taking into account the scattering at large angles and the deflection from the Born approximation are neglected. It deals with restrictions on calculation time and intrinsic numerical difficulties to implement the Molière or most accurate Goudsmit-Saunderson probability distributions [4,5]. The effect of distant scattering accumulated on some length L can be considered in the following approach. The electron undergoes a large number of statistically independent elastic collisions whose bulk effect can be determined in terms of the square of the mean deflection

$$\langle \theta^2 \rangle = N_n L \int_{\theta < \theta_{cut}} \theta^2 d\sigma_{en} \approx 8\pi \left(\frac{Ze^2}{m_e v^2} \right)^2 L \sum_i N_i \Lambda_i \quad (2)$$

with the electron Coulomb logarithm

$$\Lambda_i = \ln \frac{\theta_{cut} m_e v a_i}{\hbar} + \left(\frac{i}{Z} \right)^2 \ln \frac{0.607 a_d}{a_i}, \quad (3)$$

and i the number of various ion species in the plasma, N_i the number density of ions with charge state i , N_n the number density of the plasma nuclei, \hbar is the Planck constant, a_d the Debye radius, and a_i the effective ion radius evaluated through the ion form-factor $F(q)$

$$(Z^2 - i^2) \ln a_i = - \int_0^{\infty} \ln q \frac{\partial}{\partial q} [Z - F(q)]^2 dq, \quad (4)$$

with $\hbar q = 2m_e v \sin(\theta/2)$ the momentum transferred to the nucleus. The cutoff angle θ_{cut} which divides the distant and close scatterings is introduced. The value of this angle is taken in the range $v_0/v \ll \theta_{cut} \ll 1$, with v_0 the characteristic velocity of bound electrons. All the sub-cutoff interactions with small angular deflections (distant scatterings) are grouped statistically on some step L of the electron trajectory. The length of this step is chosen so that the Gauss approximation is valid (many collisions are occurring and the approximations of small angle theory are satisfied). The

probability that the electron accumulates the deflection angle θ on the length L due to distant scatterings is determined by the restricted Gauss multiple-scattering distribution [13]

$$P(\theta)d\theta = \frac{2\theta}{\langle\theta^2\rangle} \exp\left(-\frac{\theta^2}{\langle\theta^2\rangle}\right) d\theta. \quad (5)$$

At the end of each length L the deflection angle θ is sampled from this distribution function.

To represent the deflections of the electron by the nuclei at large angles (close scatterings) the super-cutoff part of the Rutherford cross section (eq. (1)) is used. These scatterings are treated as discrete events. The probability of these events is described by the macroscopic cross section of the elastic scattering Σ_n , which is calculated by integration of the differential Rutherford cross section (eq. (1)) in the limits from θ_{cut} up to π and multiplying by the number density of the nuclei N_n

$$\Sigma_n = N_n \int_{\theta_{cut}}^{\pi} \frac{d\sigma_{en}}{d\Omega} d\theta = \pi N_n \left(\frac{Ze^2}{m_e v^2} \right)^2 \frac{1 + \cos\theta_{cut}}{1 - \cos\theta_{cut}}. \quad (6)$$

The angle of close scattering θ is sampled from the super-cutoff part of distribution function using pseudorandom numbers

$$\frac{N_n}{\Sigma_n} \int_{\theta_{cut}}^{\theta} \frac{d\sigma_{en}}{d\Omega} d\theta = \xi, \quad (7)$$

where ξ is a random number between 0 and 1.

2.2 Electron-electron collisions

The differential cross section for the energy transfer of an electron to an electron is [12]

$$\frac{d\sigma_{ee}}{d\varepsilon} = \pi e^4 \left[\frac{1}{\varepsilon^2} + \frac{1}{(E - \varepsilon)^2} - \frac{1}{\varepsilon(E - \varepsilon)} \right] \frac{1}{E}, \quad (8)$$

with $E = m_e v^2 / 2$ the kinetic energy of the incident electron, and ε the kinetic energy of the recoil electron. There is the distinction between discrete and continuous energy losses to electrons.

The continuous energy loss of electrons in cold matter is primarily due to ionization and excitation of the electron clouds surrounding the nuclei. The formalism used to describe the statistically grouped interactions with bound electrons is the Bethe-Bloch theory of charged particle energy loss [14-16]. It assumes that each electron can be treated as if it would be bound by an average binding potential. Bounded electrons are detached by the Coulomb force impact produced by the incident electron. The sub-cutoff part of the energy loss by detachment of bounded electrons can be expressed as

$$\left(\frac{dE}{dx} \right)_{<\varepsilon_{cut}} = \int_0^{\varepsilon_{cut}} \varepsilon \frac{d\sigma_{ee}}{d\varepsilon} d\varepsilon \approx \frac{2\pi e^4}{m_e v^2} N_e \ln \left(\frac{2\varepsilon_{cut} m_e v^2}{I^2} \right), \quad (9)$$

with I the average ionization potential of the medium atoms, and N_e the number density of bounded electrons. For values of ε on the order of the atomic excitation levels, the frequencies and strengths of the atomic oscillators must be taken into account and the integration is quite complicated. On the other hand, for values of ε large enough so that the atomic electrons may be considered as free, the differential cross section of eq. (8) can be used. The cutoff energy ε_{cut} is sufficiently above the atomic excitation levels, but is still small compared to E , i.e. $I \ll \varepsilon_{cut} \ll E$.

The continuous energy losses of electrons in the plasma are divided into two groups: those bound to the plasma ions and those which constitute the free electrons. The Bethe model accounts for both ionization and excitation of the plasma ions. The collision process with the ions is one whereby either the ion is left in an excited state or it is ionized. Most of the time the ejected electron, in the case of ionization, has a small amount of energy that is deposited locally. On occasion,

however, an orbital electron is given a significant amount of kinetic energy such that it is regarded as a secondary particle called a delta-electron. The restricted electron collisional stopping power, i.e. the collisional energy loss per unit path length resulting in fractional energy transfers ε less than the cutoff energy ε_{cut} , may be expressed as the integral of the differential cross section of eq. (8) for transferring a specified amount of energy, ε , to an atomic electron. That is

$$\left(\frac{dE}{dx}\right)_{<\varepsilon_{cut}} = \int_0^{\varepsilon_{cut}} \varepsilon \frac{d\sigma_{ee}}{d\varepsilon} d\varepsilon \approx \frac{2\pi e^4}{m_e v^2} \sum_i N_e^i \ln\left(\frac{2\varepsilon_{cut} m_e v^2}{I_i^2}\right), \quad (10)$$

with I_i the average ionization potential of i -th ion species, and N_e^i the number density of the bound electrons in i -th ion. The summation is performed over all the ion species existing in the plasma. The average ionization potential is a function of the atomic structure of the stopping medium and is defined by the relation

$$\ln I_i = \frac{1}{Z-i} \sum_n f_n \ln E_n, \quad (11)$$

with E_n the energy difference and f_n the oscillator strength of transition n . This parameter is the most important characteristic in the Bethe equation that needs to be scaled with the plasma ionization. The allowed transitions change as the atoms are ionized. This implies that I_i is a function of the plasma temperature. A direct calculation of I_i from first principles is difficult, and experimental data which would allow its determination for highly ionized atoms do not exist. Therefore, these characteristics were obtained from quantum-mechanical calculations in accordance with the Hartree-Fock-Slater model [17,18].

As the plasma is heated up the contribution of free electrons to the stopping power becomes important. Free electrons are released through ionization of the ions of the plasma. This ionization increases the number of free plasma electrons which can then participate in the slowing down process and reduces the number of bound electrons. The energy loss of the incident electrons as a result of interaction with the free electrons of the plasma is calculated from

$$\left(\frac{dE}{dx}\right)_{free} = \frac{2\pi e^4}{m_e v^2} N_e^f \ln \frac{2\varepsilon_{cut} m_e v^2}{\hbar^2 \omega_p^2}, \quad (12)$$

with N_e^f the number density of the free electrons in the plasma, and $\omega_p = \sqrt{4\pi N_e^f e^2 / m_e}$ the electron plasma frequency. The number density of free electrons and the charge state of the plasma were determined in a wide range of plasma temperatures and densities by solving the Saha equations. The total energy loss can be written as the sum of the Bethe-Bloch contribution and the electronic stopping power due to free electrons

$$\left(\frac{dE}{dx}\right)_{tot} = \left(\frac{dE}{dx}\right)_{<\varepsilon_{cut}} + \left(\frac{dE}{dx}\right)_{free}. \quad (13)$$

Eventually, the energy of the primary electron is dissipated in excitation and ionization of the plasma ions and as a result of interaction with the free electrons of the plasma.

Super-cutoff interactions are close collisions of incident electrons with the plasma electrons. If this is the case, the bound electrons are assumed to be free, i.e. their atomic binding energy is ignored. Energy transfers greater than ε_{cut} can be described using the super-cutoff part of the cross section (eq. (8)). These super-cutoff interactions are treated discretely. Because of the identity of the final electrons, the cross section is symmetric with respect to the two outgoing electrons. The electron with the larger energy is, by definition, the primary. Therefore, only the range $0 \leq \varepsilon \leq E/2$ is of interest. The total macroscopic cross section Σ_e of the close electron collisions is obtained by integration of the differential cross section (eq. (8)) in the range from ε_{cut} to $E/2$ and multiplication with the number density of plasma electrons

$$\Sigma_e = \frac{\pi e^4 Z N_n}{E} \left(\frac{E - 2\varepsilon_{cut}}{E \varepsilon_{cut}} + \frac{E - 2\varepsilon_{cut}}{E(E - \varepsilon_{cut})} + \frac{1}{E} \ln \left(\frac{\varepsilon_{cut}}{E - \varepsilon_{cut}} \right) \right). \quad (14)$$

The energy of the delta-electrons is sampled from the super-cutoff differential cross section (eq. (8)) in the same way as for close electron nuclear collisions. The angle between the primary direction and the direction of the newly generated secondary electrons is determined by momentum conservation. The delta-electrons are followed separately in the same manner as primaries.

3. MONTE CARLO TECHNIQUE

For simulation of the actual physical processes a 3-D Monte Carlo approach [19-21] is used. The Monte Carlo method allows to simulate the random trajectories of electrons in the target. The Monte Carlo technique obviously provides a much better way for solving the electron transport problem, not only because all of the fundamental processes can be included, but because arbitrary geometries can be treated. In addition, other minor processes, such as photon production, can be added as a further generalization. This method is efficient for inhomogeneous plasma and in case of presence of external fields. It allows to take into account the secondary particles. Random numbers are used in the Monte Carlo method for sampling the trajectory elements (length, scattering angle) from appropriate probability distributions. Inherent variance reduction techniques have not been used, therefore fluctuations in the Monte Carlo results should represent real-life fluctuations. It is important, that the Monte Carlo method doesn't require the formulation of a discrete model of the transfer equations as is the case with analytical treatments. These generally start with a set of coupled integro-differential equations which can be solved only when using rather simplifying approximations.

3.1 Target

The plasma target is represented in the form of a cube or a parallelepiped. The coordinate frame is chosen in the following manner. It is supposed that the electron flux is incident on the plane (y, z) and propagates along the axis x into the

plasma depth. The lengths along the axes x, y, z are discretized and represented by the $I+1, J+1, K+1$ grid points x_i, y_j, z_k . It is considered the spatial mesh the points x_i, y_j, z_k of which form the cell boundaries. Thus, the cell is described by the numbers (i, j, k) . The target properties such as density, temperature and magnetic field intensity are assumed to be constant within cell (i, j, k) . The properties of adjacent cells may be different. In the present calculations the lengths along the y and z axes are set to be infinite. Thus, the plasma layer is only considered.

The magnetic field \mathbf{B} lies in the plane (z, x) . An arbitrary angle α may be given between the direction of the vector \mathbf{B} and the x axis. The Lorentz force acts the electron motion in the magnetic field \mathbf{B} . This force is perpendicular to \mathbf{B} and to the velocity \mathbf{v} of the electron. Due to this force the electron rotates around the magnetic field line with the Larmor frequency $\omega = e c B / (m_e c^2 + E)$, with c the light velocity, and E the electron kinetic energy. In the plane which is perpendicular to the magnetic field direction the electron moves along a circle with the Larmor radius $R = v_{\perp} / \omega$, where v_{\perp} is the transverse velocity component. The Larmor radius is very small and its value is varied from $2 \cdot 10^{-3}$ up to $2 \cdot 10^{-2}$ cm with the incident energy ranging from 1 up to 100 keV at $B = 5$ T. The guiding center moves along the magnetic line. The resulting trajectory is a spiral with the step $H = 2\pi v_{\parallel} / \omega$, where v_{\parallel} is the longitudinal velocity component. This spiral is twisted around the magnetic line. When entering the plasma, the electron undergoes collisions with the plasma particles and its direction changes. Thus, the values and the directions of the magnitudes v , v_{\perp} , and v_{\parallel} are changing due to collisions. After a collision the electron moves along a new magnetic field line with new values of velocity, Larmor radius and spiral step before the next collision is occurring. An example of the trajectory of the magnetized electron in the plasma is presented in Fig. 1. After the first collision the electron moves in the back direction along the new magnetic field line. Generation of the secondary electron is also illustrated.

3.2 Sampling parameters of incident electrons

The initial energy of the incident electron can be monoenergetic or Maxwellian distributed. The two-dimensional Maxwellian function in terms of the velocity components can be written in the form

$$f(v_x)dv_x = \sqrt{\frac{m_e}{2\pi T}} \exp\left(-\frac{m_e v_x^2}{2T}\right) dv_x, \quad f(v_z)dv_z = \sqrt{\frac{m_e}{2\pi T}} \exp\left(-\frac{m_e v_z^2}{2T}\right) dv_z, \quad (15)$$

with T the electron temperature, and v_x and v_z the velocity components along the axes x , and z . Using the substitutions

$$x^2 = m_e v_x^2 / 2T, \quad z^2 = m_e v_z^2 / 2T \quad (16)$$

and multiplying eq. (15) the following expression is obtained

$$f(x, z) dx dz = \frac{1}{\pi} \exp(-x^2 - z^2) dx dz. \quad (17)$$

This expression may be written in the polar coordinate system in the form

$$f(r, \phi) dr d\phi = \frac{1}{\pi} \exp(-r^2) dr^2 d\phi, \quad (18)$$

with the substitutions

$$x = r \cos \phi \quad \text{and} \quad z = r \sin \phi. \quad (19)$$

The coordinates r and ϕ are independent. Therefore, the values r and ϕ may be sampled according to

$$\frac{\int_0^\phi f(\phi) d\phi}{\int_0^{2\pi} f(\phi) d\phi} = \xi_1, \quad \frac{\int_0^r f(r) dr}{\int_0^\infty f(r) dr} = \xi_2, \quad (20)$$

where ξ_1 and ξ_2 are random numbers distributed uniformly in the interval $[0,1]$. Solving eq. (20) with respect to r and ϕ results in

$$\phi = 2\pi\xi_1, \quad r = \sqrt{-\ln \xi_2}. \quad (21)$$

This method of sampling the values r and ϕ from eq. (20) is the reverse function method. Substitution of eq. (21) into eq. (19) gives

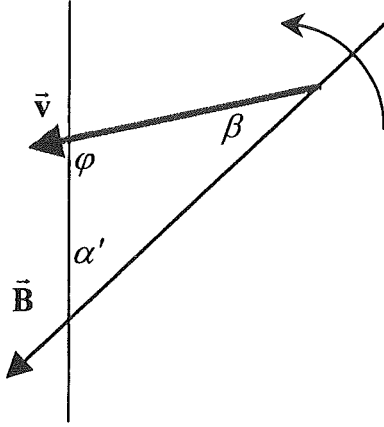
$$x = \sqrt{-\ln \xi_2} \cos(2\pi\xi_1), \quad z = \sqrt{-\ln \xi_2} \sin(2\pi\xi_1). \quad (22)$$

The energy components of the electrons are calculated from eq. (19) as $E_x = Tx^2$ and $E_z = Tz^2$. The incident electron energy is $E = E_x + E_z$.

Electrons with high energy (tail of the Maxwellian distribution) are occurring with low probability. However, these electrons influence essentially the tail of the distribution of absorbed energy in the target. To increase the fraction of high energy electrons the scheme with "weight" is used. The electron energy components E_x and E_z are sampled uniformly in the interval $[E_1, E_2]$ in accordance with the expressions $E_x = E_1 + \xi_1(E_2 - E_1)$ and $E_z = E_1 + \xi_2(E_2 - E_1)$. The incident energy is $E = E_x + E_z$. The "weight" of the electron is determined by the following expression

$$P(E_x, E_z) = \frac{4(E_2 - E_1)}{\pi T \sqrt{E_x E_z}} \exp\left(-\frac{E_x}{T} - \frac{E_z}{T}\right). \quad (23)$$

As a result of collisions and stopping, the electron loses the energy ΔE . This energy is placed into a cell in which the collisions and stopping were taken place with calculated "weight" P , i.e. the absorbed energy in a cell is $P \cdot \Delta E$. The sum of the values $P_n E_n$ over all the histories gives the average energy of the incident electron flux $\sum_n P_n E_n = \langle E \rangle$, where E_n and P_n are the sampled electron energy and the electron "weight" for the n -th history.



The initial angle of the incident electron with the plasma surface may be fixed or sampled from an arbitrary distribution function. In case of magnetized electrons, the trajectory is a spiral with the Larmor radius R . The start of the trajectory is sampled randomly on the circle with radius R . The initial electron energy can be presented as the sum of the longitudinal and the transverse energy components $E = E_{\parallel} + E_{\perp}$. The impact angle (let us denote it by

means φ) is a function of the angle between the magnetic field direction and the plasma surface, α' , and the pitch angle between the magnetic field direction and the electron velocity direction, β . The longitudinal kinetic energy E_{\parallel} is a function of the pitch angle $E_{\parallel} = E \cos^2 \beta$. There are two possible cases for the impact angle of the electron: 1) $E_{\parallel} = E$; 2) $0 \leq E_{\parallel} < E$. It is evident that in the first case the pitch angle $\beta = 0$. If this is the case, the impact angle φ with the plasma shield is always equal to α' , i.e. the electron moves along the magnetic field line. In the second case, it is supposed that the pitch angle β is isotropic in the interval $0 < \beta \leq \pi/2$ relating the direction \vec{B} . The pitch angle is sampled randomly in the interval $[0, \pi/2]$ using the expression $\beta = \xi \cdot \pi/2$ with the random number ξ uniformly distributed in the interval $[0, 1]$. When β approaches $\pi/2$ the electron trajectory is a circle around the magnetic line. In the second case, the impact angle φ with the plasma shield is found in the range from 0 up to $180 - (\alpha' + \beta)$, when $\alpha' + \beta > 90$ or $90 - (\alpha' + \beta)$, when $\alpha' + \beta < 90$. When φ approaches zero the electron trajectory touches the plasma surface. Let us imagine that we rotate the vector \vec{v} around \vec{B} and move it along \vec{B} . The end point of \vec{v} will move along a helix. This helix will cross several times the plasma shield surface before full immersion occurs. Thus, the electron enters and exits the target many times. In the Monte Carlo model the angle φ is not specified beforehand accept the case when $\varphi = \alpha'$. The simulation procedure of the entrance of the electron into the target is the following: Outside of the target, the circle with the Larmor radius is taken, which is in the plane perpendicular to the direction \vec{B} . The start of the electron trajectory is sampled randomly on this circle.

The electron moves along a helix. The radius and the step of the helix depends strongly on the longitudinal kinetic energy E_{\parallel} which is a function of the pitch angle β . The pitch angle is specified beforehand or is sampled isotropically in the interval $[0, \pi/2]$. When E_{\parallel} is close to zero the electron is strongly rotating around the magnetic line. At the impact with the plasma shield the angle of entrance will be found in the range pointed above. Before the full entrance, the electron crosses the target surface many times, especially, with small E_{\parallel} . This simulation procedure describes the actual situation that exists near the target. In case of a plasma shield as target the edge of the plasma shield is the low-density plasma (about 10^{16} cm^{-3}). In such plasma the distance between two consequent close collisions (collisions in which the electron direction is changed) is much greater than the step of the helix. Thus, the electron penetrates into the plasma shield on a significant depth without close collisions (on this path the continues energy loss due to distance collisions is taken into account). The fraction of energy deposited into graphite will depend on the degree of electron rotating before the high-density plasma near the graphite surface. When the electron is not rotating ($E_{\parallel} = E$) the penetration depth will be maximum. Thus, the impact angle on the plasma shield has minor influence on the energy deposition profile. The energy deposition depends significantly on the ratio of the longitudinal energy to the total kinetic energy (the degree of rotating) before the fraction of the dense plasma shield.

3.3 Macroscopic cross sections

The total macroscopic cross section Σ_t is determined as the sum of the electron nucleus Σ_n (eq. (6)), the electron electron Σ_e (eq. (14)), and a fictitious cross section Σ_f . The cross section Σ_t determines the mean "free path" length L between two close collisions. In case of an inhomogeneous plasma, the mean "free path" changes as the electron moves from one cell to another with different properties. Due to continuous energy loss, the cross section varies along the path of the electron. In addition, the electron is no longer gyrating. The "free path" length

between two close collisions is sampled randomly. To take into account large lengths the Monte Carlo technique of the fictitious process [22] is applied. An additional fictitious interaction is introduced which, if it occurs, results in straight-ahead scattering (i.e., no interaction at all). The macroscopic cross section of this process is calculated as $\Sigma_f = (dE/dx)_{cut} / (0.01E)$, where $(dE/dx)_{cut}$ is the sub-cutoff part of restricted electron collision stopping power, E is the energy of the electron at the start of given "free path" step. Thus, the probability of the fictitious process is determined so that the energy loss per "free path" step is 1% of the kinetic energy at the start point of this step. In case, the fictitious process occurs the energy and direction of the electron is not changed. This algorithm allows to use large "free path" steps and to save computing time.

3.4 Electron transport algorithm

In case of an inhomogeneous plasma shield there are gradients of density, temperature and magnetic field. To simulate the electron path length in such a medium the approximation of the plasma with segment-constant characteristics is used. The space in which the simulation takes place is divided into a finite number of regions (i layers) in each of which the plasma is homogeneous and of constant density, temperature and magnetic field intensity. The algorithm for simulation of the path length in an inhomogeneous plasma with segment-constant characteristics assuming the magnetized electron propagates from the point r_0 in the direction Ω is the following

1. The random value of the optical path length is sampled according to $s = -\ln \xi$.
2. The total macroscopic cross section $\Sigma_i^{i,j,k}$ is calculated as described above for the (i, j, k) -th cell in which the point r_0 is located.
3. The spiral length d to the nearest cell boundary is determined in the direction Ω .
4. The optical thickness d^{opt} is evaluated from the expression $d^{opt} = \Sigma_i^{i,j,k} d$.
5. If $s \leq d^{opt}$, then the coordinates of the collision point are calculated as

$$\begin{aligned}
x_1 &= c_x + HL \cos \alpha / L_i - R [\cos(2\pi L / L_i) \cos \varphi_z - \sin(2\pi L / L_i) \sin \varphi_y] \sin \alpha, \\
z_1 &= c_z + HL \sin \alpha / L_i + R [\cos(2\pi L / L_i) \cos \varphi_z - \sin(2\pi L / L_i) \sin \varphi_y] \cos \alpha, \\
y_1 &= c_y + R [\sin(2\pi L / L_i) \cos \varphi_z + \cos(2\pi L / L_i) \sin \varphi_y],
\end{aligned} \tag{24}$$

with c_x, c_y, c_z the center coordinates of the Larmor circle, $L = s / \Sigma_i^{i,j,k}$ the spiral "free path" length up to the collision point, $L_i = 2\pi v / \omega$ the spiral period length, α the angle between the magnetic field and axis x directions, φ_z the initial phase of the electron with the axis z , and φ_y the initial phase of the electron with the axis y . Eq. (24) is written for the case when the vector \mathbf{B} of magnetic field is in the plane (z, x) and has the angle α with direction of the axis x . On the "free path" length L , the energy loss is taken into account in the (i, j, k) -th cell in accordance with $\Delta E_{i,j,k} = L(dE/dx)_{tot}$, where $(dE/dx)_{tot}$ is described by eq. (13). In the end of the length L the new direction cosines $\alpha_1, \beta_1, \gamma_1$ are calculated with account of the small deflection angle θ sampled from eq. (5) by as follows

$$\begin{aligned}
\alpha_1 &= \alpha_0 \cos \theta + (\alpha_r - \alpha_0 \cos \theta_r) \sqrt{(1 - \cos^2 \theta) / (1 - \cos^2 \theta_r)}, \\
\beta_1 &= \beta_0 \cos \theta + (\beta_r - \beta_0 \cos \theta_r) \sqrt{(1 - \cos^2 \theta) / (1 - \cos^2 \theta_r)}, \\
\gamma_1 &= \gamma_0 \cos \theta + (\gamma_r - \gamma_0 \cos \theta_r) \sqrt{(1 - \cos^2 \theta) / (1 - \cos^2 \theta_r)},
\end{aligned} \tag{25}$$

with $\alpha_0, \beta_0, \gamma_0$ the initial direction cosines with coordinate axes in the collision point, $\alpha_r, \beta_r, \gamma_r$ the direction cosines of the random vector in space which has the uniform probability distribution, and $\cos \theta_r$ the angle cosine between the initial direction and the random vector in the collision point. The simulation of the spiral path length is finished.

6. If $s > d^{opt}$ and the electron is within the boundaries of the target, then the new values of s and Σ_i are calculated $s = s - d^{opt}$, $\Sigma_i = \Sigma_i^{i',j',k'}$ where $\Sigma_i^{i',j',k'}$ is the macroscopic cross section for a new cell which the electron is crossing. The new coordinates of the point on the cell boundary are evaluated by means of eqs. (24) where instead "free path" length L the value d is used. The energy loss and

correction of the direction cosines are performed on the length d as described above. After that, the simulation is continued from the item 3.

7. If $s > d^{opt}$ and the electron crosses any target boundary, then the energy loss is taken into account on the length d and the electron trajectory is stopped.

The length d to the nearest cell boundaries in the target is calculated from a joint solution of eqs. (24) for a spiral and those for boundary planes.

Because a "free path" step represents the cumulative effect of many individual random collisions, fluctuations in the energy loss rate will occur. The technique presented above takes into account these fluctuations in any particular segment of the path. The restricted-collision stopping power technique allows to avoid the implementation of the Landau energy-straggling distribution [10,11], and to predict successfully the energy transfers.

3.5 Sampling electron interactions

When a point of close interaction has been reached, it must be decided which of the competing processes has occurred. The probability that a given type of interaction occurred is proportional to its cross section. The type of interaction in the collision point can be the following 1) *elastic electron nucleus collision*; 2) *elastic electron electron collision*; 3) *ficitious process*. Suppose the types of interactions possible are numbered 1 to 3. Selection of the i -th type of interaction is made randomly according to the probability $f(i) = \frac{\sum_{i=1}^3 \Sigma_i}{\Sigma_i}$. The number of the interaction to occur, i , is selected by picking a random number ξ and finding the i which satisfies $f(i-1) < \xi < f(i)$.

1) Close electron nucleus collisions

This process gives the main contribution into the scattering of electrons in the plasma. The differential cross section of this process is described by eq. (1). The scattering angle θ in the laboratory frame is sampled from this expression by means of the reverse function method. The energy transferred to the nucleus is determined from the expression

$$\Delta E = 4 \frac{m_e M_n}{(m_e + M_n)^2} E \sin^2 \frac{\theta}{2} \quad (26)$$

with E the kinetic electron energy before the collision, and M_n the nucleus mass. The electron energy will be less by this value after scattering. The criterion of the trajectory end in the energy is checked. If the electron energy is less than the threshold energy $E_{th} = 1$ keV, then the trajectory is stopped and a new trajectory is started. Otherwise, the electron trajectory is traced with the new electron energy and new direction cosines.

2) Close electron electron collisions

The energy ε transferred to the recoil electron in close collisions is sampled from eq. (8) by means of the method of inverse functions. The cosine of the scattering angle θ in the laboratory frame is evaluated from the expression $\cos\theta = \sqrt{1 - \varepsilon/E}$. The recoil electrons can obtain energies higher the threshold energy $E_{th} = 1$ keV. If this is the case, their trajectories are followed in the similar way. When the electron energy is smaller than E_{th} , the trajectory is stopped. In opposite way, the simulation procedure is repeated with new values of the electron energy and direction.

3) The fictitious process

The fictitious collision is occurred with the probability Σ_f/Σ_t . If one takes place, then the electron energy and direction are not changed.

Thus, Monte Carlo simulation is performed by carrying out the above calculation on many test electrons.

3.6 Evaluation of the distribution of energy deposition

As a result of N histories, there are some values of absorbed energy $\Delta E_{i,j,k}$ [keV] in each cell (i, j, k) . In order to determine the energy $\Delta \varepsilon_{i,j,k}$ [keV] per electron, it is necessary to divide the values $\Delta E_{i,j,k}$ by the number of histories N . Considering

slab geometry the lengths along the axes y and z are assumed to be infinite. The energy $\Delta\varepsilon_i$ [keV] per electron in the i -th layer is evaluated by taking the sum with respect to all the values $\Delta\varepsilon_{i,j,k}$ [keV] for the given i -th index, i.e. the summation is performed over all the j -th and k -th indexes. Dividing each value $\Delta\varepsilon_i$ [keV] by the grid step h_i [cm] one can obtain the deposited energy (dE/dx) [keV/cm] per electron along the axis x . This value was averaged over different collisional histories. Thus, it can be treated as the power density (dQ/dx) [keV/(cm³·s)] for the incident flux $F = 1$ [electrons/(cm²·s)] before the target. In case of monoenergetic flux, the energy density P [keV/(cm²·s)] of the incident flux and the electron energy E [keV] are the initial parameters. The incident electron flux before the target is determined as $F = P/E$ [electrons/(cm²·s)]. For hydrodynamic problems, the power density (dQ/dx) [keV/(cm³·s)] is required. To calculate this characteristic, it is necessary to multiply the value (dE/dx) [keV/cm] by the flux F [electrons/(cm²·s)] before the target.

In case of a Maxwellian flux, the initial electron energy E is sampled from the Maxwellian function $f_m(v)$. The average flux is given by $F = \int_0^\infty nvf_m(v)dv$, where $n = P/vE$ is the number density of the electrons in the incident flux. To determine the power density (dQ/dx) [keV/(cm³·s)] for the Maxwellian distributed electrons, it is necessary to multiply (dE/dx) [keV/cm] by the calculated flux F .

3.7 Accuracy of the Monte Carlo calculations

There are two main sources of error in calculations of this type. The first is statistical depending on the finite number of samples. The second is systematic arising from inaccuracies in the scattering data used.

Due to the statistical nature of the Monte Carlo method, the accuracy of the results will depend on the number of samples. Generally, the statistical uncertainties will be proportional to the inverse square root of the number of histories. Thus, to cut uncertainties in half it is necessary to run four times as many histories. For some quantities x the average is evaluated as

$$x_m = \frac{1}{N} \sum_{i=1}^N x_i,$$

where N is the number of followed histories, x_i is the quantity x on i -th history. The probability of deviation from the quantity x_m can be written as

$$P(|x_m - x_a| < z_\beta \sqrt{D(x)/N}) \approx \beta, \quad (27)$$

with x_a the accurate value of x , $D(x)$ the dispersion, β the coefficient, and z_β the root of the equation $F(z) = \beta$. Here $F(z)$ is the error integral. The probable error corresponds to the coefficient $\beta = 0.5$. In this case, the value z_β is equal to 0.6745.

Therefore, the value x_a is found in the range

$$x_m - 0.6745 \sqrt{D(x)/N} \leq x_a < x_m + 0.6745 \sqrt{D(x)/N}, \quad (28)$$

with

$$D(x) = \frac{N}{N-1} \left[\left(\frac{1}{N} \sum_{i=1}^N (x_i)^2 \right) - (x_m)^2 \right]. \quad (29)$$

This simple approach was used in the Monte Carlo calculations to evaluate the statistical error in the distribution of energy deposition. The error was investigated by repeating the calculations using a different set of trajectories and its number. The accuracy increases only as the square root of the number of trajectories considered. In the present calculation 10000 trajectories were used. The ultimate accuracy can be set by the available computer time. It was found that this number of histories is sufficient because the statistical error then is less than the error arising from other sources.

The accuracy of the Monte Carlo calculations depends on the accuracy of the interaction cross sections. The differential cross section of elastic electron nucleus scattering (eq. (1)) was derived in the first order Born approximation. The spin and screening effects are not taken into account by this formula. The error introduced by this cross section is of the order of 20% in the energy range of interest here. For a significant increase in accuracy, it would be necessary to use the exact Mott cross

section [23] which takes into account the above effects. However, this would involve a considerable increase in the complexity of the computer programs and in their running time. The error introduced by the cross section for energy transfers (eq. (8)) makes a few percent.

Also, for given cutoff angles and energies, the computer time for an electron history is slightly more than linear in the energy of the incident electron. The point to be made here is that Monte Carlo calculations can be very time consuming.

4. NUMERICAL RESULTS

The three-dimensional Monte Carlo code MONPLAS has been developed to describe the transport of magnetized electrons in solid targets and in a carbon plasma.

4.1 Energy deposition into solid targets

In solid targets, the magnetic field has no influence on the electron trajectory as the free path length between two collisions is much less than the Larmor radius. Therefore, the electron undergoes a set of collisions during one Larmor period. Due to the collisions, the electron direction is deflected and it moves around another magnetic line. The trajectory length between two collisions is approximately a direct line. However, the energy deposition profile depends strongly on the value of the longitudinal kinetic energy E_{\parallel} of the electrons at the entrance into the target. In Fig. 2 distributions of the energy deposition into a graphite target are presented for different longitudinal energies E_{\parallel} . The electrons in the incident flux are Maxwellian distributed with a temperature of 10 keV. The two-dimensional Maxwellian function is shown in Fig. 2. The energy of the incident electrons is sampled from this function. The scheme with weight is applied for accurate account of the energy deposition by the high energy electrons from the tail of the Maxwellian distribution. Fig. 3 shows results for magnetic field lines perpendicular to the target surface (entrance angle 90°). The magnetic field intensity is equal to 5 T. The energy deposition decreases monotonically with the target depth. The range of the high energetic tail of the

Maxwellian distributed electrons is up to 80 μm . Low-energy electrons deposit its energy near the target surface. Energy and angular spectra of Maxwellian electrons reflected from graphite are shown in Figs. 4 and 5, respectively. With decreasing longitudinal energy the fraction of reflected electrons increases and the maximum in the angular distribution is shifted close to the target surface. The angle is accounted from the direction of the x axis. For a case when the rotational motion is absent (the longitudinal energy is equal to the incident one) the most probable angle of the backscattered electrons is about 135° that is a well-known result. Fig. 6 shows distributions of the energy deposition for a case when the magnetic field lines form an angle of 5° with the target surface. Decrease in the entrance angle results in shift of the energy deposition towards the target surface. The range of energy deposition into graphite decreases up to 60 μm . The differences in the energy deposition curves for different longitudinal energies are less pronounced in comparison with the previous case. Figs. 7 and 8 show energy and angular spectra of the reflected electrons for a case when the magnetic lines form an angle of 5° with the target surface. In this case the fraction of backscattered electrons with $E_{\parallel} = E$ is dominant. The most probable angle with the target surface ranges from 5° to 10° for all the longitudinal energies.

4.2 Energy deposition into a homogeneous carbon plasma

Calculated distributions of the energy deposition versus the longitudinal kinetic energy of the monoenergetic incident electrons are shown in Fig. 9. A layer of homogeneous carbon plasma with density 10^{19} cm^{-3} and temperature 20 eV was considered. The monoenergetic energy E of incident electron flux was assumed to be 50 keV. The magnetic field is equal to 5 T. Magnetic field lines are perpendicular to the plasma layer. Monte Carlo calculations were performed for five values of the longitudinal kinetic energy E_{\parallel} , which was taken 50, 30, 20, 10 and $E \cos^2 \theta$ keV with θ the isotropic pitch angle. The peak of the energy deposition is shifted to the plasma surface for the incident electron flux with lower longitudinal energy. For the case of isotropic pitch angle and monoenergetic energy a maximum in the energy deposition is achieved on the plasma surface.

The magnetic field has no influence on the distribution of the energy deposition for the same ratios of longitudinal to transverse energies at constant total energy as is seen from Fig. 10 showing the distributions of the energy deposition for given values of the longitudinal kinetic energy and different values of the magnetic field. The total monoenergetic energy of the incident electrons E is equal to 40 keV. The calculations were performed for longitudinal kinetic energies $E_{\parallel} = E$, $E_{\parallel} = 0.5E$, $E_{\parallel} = 0.1E$, $E_{\parallel} = E \cos^2 \theta$ with θ the isotropic pitch angle and for magnetic field with 0.1, 1, 10, and 100 T, respectively. The energy distributions depends only on the value of the longitudinal energy. This result can be explained as follows: the magnetic field has an effect only on the electron trajectory (motion along a spiral), but has no influence on the collision probability, value of transferred energy, path length between two consequent collisions, and energy loss on this length. Therefore, for given ratios of longitudinal to transverse energy the distribution of energy deposition should not depend on the magnetic field.

Fig. 11 shows the energy deposition as a function of the entrance angle of the electrons into the carbon plasma. The angle is formed by the magnetic field lines with the x axis, which is perpendicular to the plasma surfaces. Magnetic field is 5 T. The plasma density is 10^{19} cm^{-3} . Plasma temperature is 20 eV. Monoenergetic energy of the incident electrons is 50 keV. The longitudinal kinetic energy of the electrons is equal to the total energy, i.e. the electrons are not rotating, and they move along the magnetic field lines. The calculations were performed for four values of the angle between the magnetic field lines and the x axis. From Fig. 11 it is seen that with increasing angle, the penetration depth of the electrons into the plasma is strongly decreased and the energy deposition close to the plasma surface is higher.

Distributions of the energy deposition as a function of the carbon plasma temperature are shown in Fig. 12. The plasma density is equal to 10^{18} cm^{-3} . The total monoenergetic energy of the incident electrons is 50 keV. The longitudinal kinetic energy is equal to the total one. The magnetic field is 5 T. Magnetic field lines are perpendicular to the plasma surface. The calculations were performed for four values of the plasma temperature. As can be seen from Fig. 12 the penetration depth of the electrons into the plasma decreases with temperature increase and the displacement of energy deposition peak to the plasma surface occurs. This can be explained by the

following: with increasing temperature the ionization of the plasma increases, accordingly, the energy losses on the free plasma electrons are increased.

Fig. 13 shows energy deposition profiles for monoenergetic and Maxwellian distributed electrons. The carbon plasma density is 10^{19} cm^{-3} and its temperature is 20 eV, the magnetic field is 5 T with the magnetic lines perpendicular to the plasma surface. The monoenergetic electrons have the energy $E=50 \text{ keV}$ and its longitudinal energy $E_{\parallel}=0.5E$. The initial energy of the Maxwellian distributed electrons E_m is sampled from a two-dimensional function. The temperature of the Maxwellian distributed electrons was also taken as 50 keV. Two cases are considered. It is supposed that the longitudinal kinetic energy equals half of the total energy $E_{\parallel}=0.5E_m$ and $E_{\parallel}=E_m \cos^2 \theta$ with θ the isotropic pitch angle. From a comparison of the distributions of energy deposition it is evident that the penetration depth of the Maxwellian electrons exceeds significantly that of the monoenergetic ones. The distribution of energy deposition of the Maxwellian electrons has a long tail contributed from high-energy Maxwellian electrons. Energy deposition profile with $E_{\parallel}=E_m \cos^2 \theta$ is close to that with $E_{\parallel}=0.5E_m$.

Distributions of the energy deposition as a function of the incident energy of the electrons are shown in Fig. 14. Parameters of the plasma are the following: density 10^{19} cm^{-3} and temperature 20 eV. The magnetic field is 5 T and the field lines are perpendicular to the plasma surface. The longitudinal energy is equal to the total one. The calculation was performed for the following values of the total monoenergetic energy of the incident electrons: 10, 20, 40 and 80 keV. The energy deposition decreases with increasing impact energy. A variation of the incident energy from 10 up to 80 keV changes the penetration depth into a plasma by a factor of 50.

Distributions of the energy deposition for different densities of a plasma are presented in Fig. 15. The plasma temperature is 20 eV. Intensity and direction of the magnetic field are the same as in the previous case. The total monoenergetic energy of the incident electrons is 50 keV. The longitudinal kinetic energy is equal to the total one. The calculations were performed for five values of the plasma density: 10^{16} , 10^{17} , 10^{18} , 10^{19} and 10^{20} cm^{-3} . With decreasing the plasma density by an order of

magnitude the penetration depth increases by about a factor of 10. The energy deposition decreases by several orders with decreasing the plasma density.

4.3 Energy deposition into graphite shielded by a carbon plasma layer

Calculations on the energy deposition of the magnetized electrons into a two-phase target consisting of a homogeneous plasma layer of thickness of 20 cm and a graphite material shielded by this layer were also carried out. It is supposed that the incident electrons in the flux are Maxwellian distributed in energy with the temperature of the electron flux as 10 keV. Results of the energy deposition into a homogeneous plasma and graphite shielded by this plasma are shown in Figs. 16 and 17, respectively. A homogeneous plasma of density of 10^{18} cm^{-3} and of temperature of 5 eV is considered. The magnetic field is 5 T and the field lines are perpendicular to the plasma surface. The curves in Figs. 16 and 17 correspond to different values of the longitudinal kinetic energy of the incident Maxwellian electrons. Figs. 18 and 19 show results for magnetic field lines forming an angle of 5° with the plasma surface. The calculations are also carried out for four values of the longitudinal kinetic energy of the Maxwellian electrons. As it is seen from Figs. 16 and 18 the energy deposition profiles have a peak close to the plasma surface. The most probable energy of the Maxwellian electrons is approximately equal to 10 keV. Therefore, the main fraction of the electrons has this energy. Electrons with energy close to the most probable one are absorbed near the plasma surface. Thus, the peak in the distribution of the energy deposition into carbon plasma is due to the electrons of this energy. For the case of an angle of 5° the energy deposited close to the plasma surface is higher by about a factor of 4. Some part of the energy of the high energetic tail of the Maxwellian distributed electrons is deposited into the graphite target. The fraction of high-energy Maxwellian electrons is small. However, the action of these electrons is significant because they deposit energy into a thin layer of graphite. For the case of perpendicular incidence (Fig. 17) the percentage of the energy deposited into graphite is 25.8%, 20.1%, 20.8%, and 13.8% for four values of the longitudinal energy $E_{\parallel} = E$, $E_{\parallel} = 0.5E$, $E_{\parallel} = E \cos^2 \theta$, and $E_{\parallel} = 0.1E$, respectively. The penetration depth into graphite is about 60 μm . If the magnetic field

lines form an angle about 5° with the plasma surface a larger fraction of the energy of the electron flux is deposited into the plasma. In this case, the percentage of the energy deposited into graphite (Fig. 19) is 0.5%, 0.26%, 0.3%, and 0.1% for four longitudinal energies. The penetration depth of the high energetic Maxwellian electrons into graphite decreases up to 40 μm .

The following examples demonstrate more realistic cases of the distributions of energy deposition of the rotating electrons into the carbon plasma with density and temperature profiles and into graphite divertor shielded by this plasma. Density and temperature profiles in the plasma for three times are shown in Figs. 20 and 21. The shielding plasma is a two-layer plasma with high density (up to 10^{19} cm^{-3}) and low temperature close to the target and low density (around 10^{15} cm^{-3}) and high temperature (up to a few hundred eV) further away [2]. Results on distribution of the energy deposition are shown in Figs. 22-29 for the plasma shield and graphite. Figs. 22-29 show the energy deposition profiles for specified longitudinal energies at 5.73, 22.66, and 101.0 μs . Figs. 24-29 show these profiles for specified times and different longitudinal energies. It is assumed that the magnetic field is constant and its components are $B_x(x) = 0.5 \text{ T}$ and $B_z(x) = 5 \text{ T}$. Thus, the direction of magnetic field is also constant and makes an angle of 5° with the plasma surface. The average percentage of energy absorbed in the plasma shield graphite target system is 81%, 83%, and 85% for three times, respectively. Thus at later times the fraction of reflected energy from the plasma shield decreases. Fig. 24, 26 and 28 shows that there is a peak in the energy deposition into the plasma. This peak results from the deposition of the magnetized electrons into the transition region of the evolving plasma shield. The energy fractions absorbed in the plasma shield are 91%, 98%, and 99.8% for three times, respectively (Fig. 22). Thus the plasma shield screens effectively the graphite divertor from the direct action of the incident electron flux, especially, at later times. The most probable energy of the Maxwellian distributed electrons is approximately from 1 to 10 keV. These electrons are absorbed close to the surface of the expanding plasma shield. A maximum in the distribution of the energy deposition on the plasma edge is due to the contribution of electrons of those energies.

For graphite, it is assumed a constant density ($\sim 10^{23} \text{ cm}^{-3}$) and room temperature. A maximum in the energy deposition (Figs. 25, 27, and 29) is achieved

on the graphite surface and the penetration depth decreases up to 40 μm at later times. Small fractions of the energy (9%, 2%, and 0.2% for isotropic pitch angle and three times, respectively (Fig. 23)) are deposited into a thin surface layer of graphite. From Fig. 25 it is seen that the depth of the energy deposition is up to 60 μm . At 101 μs the fraction of energy deposited into solid graphite is about a factor of 50 less than at 5.73 μs . The distributions of the deposited energy integrated along the distance from graphite for the plasma shield and along the depth into graphite are shown in Figs. 30-37. Figs. 30 and 31 show the integrated profiles for specified longitudinal energies as in the case of energy deposition profiles. These integrated profiles for specified times are shown in Figs. 32-37. It is evident that discrepancy in the curves for the plasma shield (Figs. 32, 34 and 36) is not so large as for graphite (Figs. 33, 35 and 37). It is seen that for graphite target after 20 μm the curves become approximately constant, i.e. the energy deposited at the distance larger 20 μm is negligible. For the case of the longitudinal energy with isotropic pitch angle the angular and energy spectra of the Maxwellian distributed electrons transmitted through the plasma shield before their impact onto graphite are shown in Figs. 38 and 39, respectively. For other longitudinal energies these spectra are similar to those. The most probable angle of the electron impact is about 90° with the graphite surface. The number of electrons with the energy from 1 keV up to 10 keV which reach the graphite surface is rather small compared to that with higher energy. Therefore, only electrons of the Maxwellian tail can penetrate through the plasma shield and impact onto the graphite plate. With ongoing time, the peak of the energy spectra decreases and shifts to higher energies as the size of the plasma shield increases. It is also assumed that impacting electrons are reflected from the plasma shield. The pitch angle can take a value greater 90° due to collisions with the plasma nuclei. If this is the case, the electrons move along the helix in backward direction and can leave the plasma shield. Such electrons are considered as reflected. Further, the reflected electrons are bended back to the plasma shield because of guiding magnetic field. Angular and energy spectra of the electrons reflected from the plasma shield are shown in Figs. 40 and 41 for a case of the longitudinal energy with the isotropic pitch angle. The probable angle of the reflected electrons is close to 90° with the plasma surface. The main fraction of the backscattered electrons is low-energy electrons in the range from 1 up to 30 keV.

5. CONCLUSIONS

The Monte Carlo method was applied to the calculation of the energy deposition of magnetized electrons in inhomogeneous plasmas and in solids to study the energy deposition of the magnetized electrons into the carbon plasma with density and temperature gradients. The study of the energy deposition may be summarized in the following set of conclusions.

- ◆ In graphite, the magnetic field has no influence on the electron trajectory because the free path is significantly less than the Larmor period length. The distribution of the energy deposition depends strongly on the longitudinal kinetic energy of the electrons before the entrance into graphite.
- ◆ The peak of energy deposition profile is close to the plasma surface and range shortening occurs with decreasing the longitudinal kinetic energy.
- ◆ The magnetic field intensity has no influence on the distribution of the energy deposition into the homogeneous plasma for the same ratios of longitudinal to transverse flux energies at constant total energy.
- ◆ Increasing the entrance angle of the electrons into the homogeneous plasma, the penetration depth is strongly decreased.
- ◆ The penetration depth of Maxwellian electrons into the plasma exceeds significantly that of the monoenergetic flux (temperature of Maxwellian electrons is equal to monoenergetic energy).
- ◆ The results of calculations indicate that electron range shortening occurs in a hot plasma layer due to the temperature, density, and incident energy dependence of the energy loss processes.
- ◆ The penetration depth and the fraction of the absorbed energy deposited into graphite shielded by a layer of homogeneous plasma increases with increasing longitudinal electron energy and entrance angle.
- ◆ The fraction of energy deposited into the evolving plasma shield increases more than 99% at later times and only the electrons from Maxwellian tail can reach the bulk target. The depth of significant energy deposition into graphite shielded by a

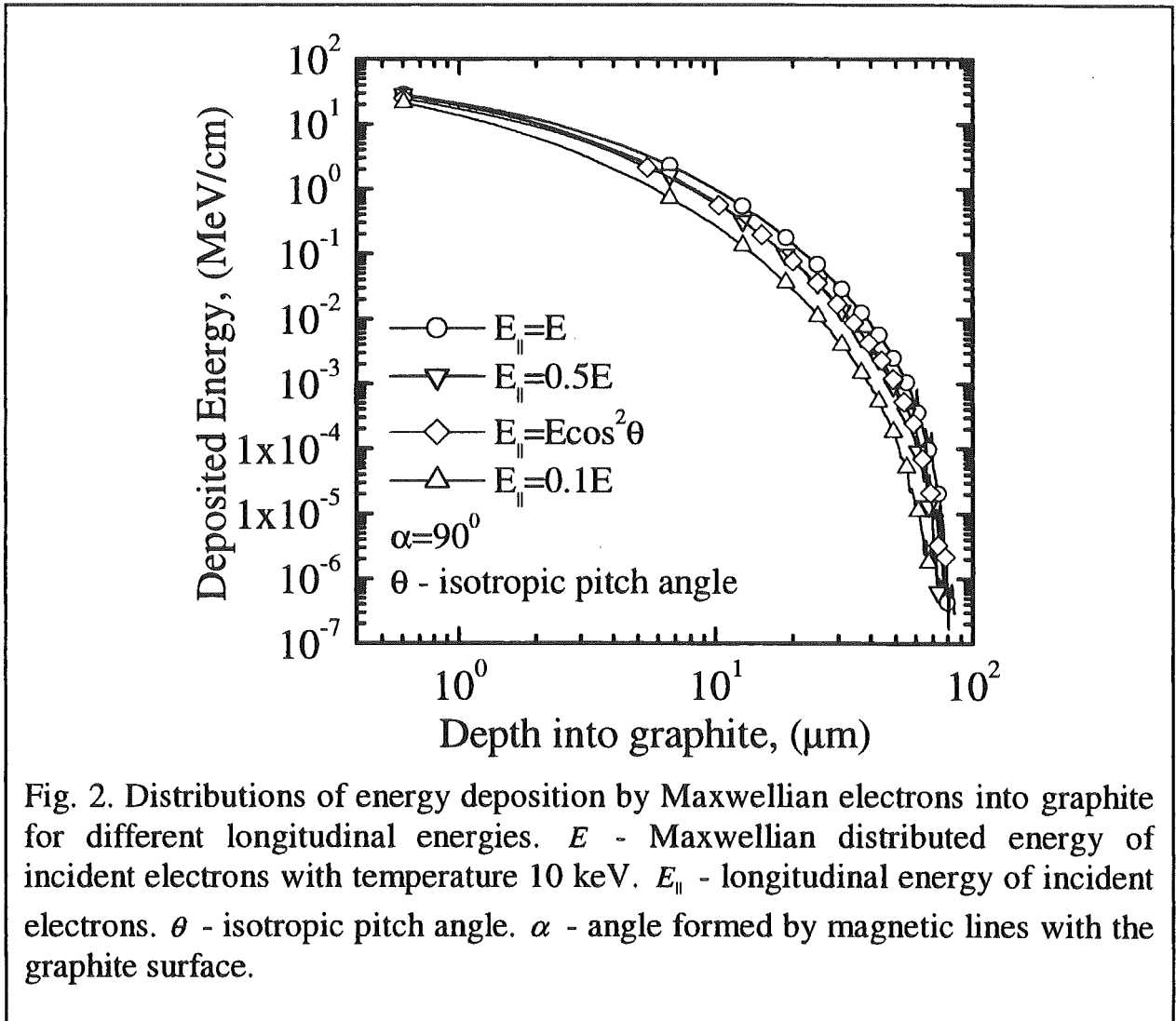
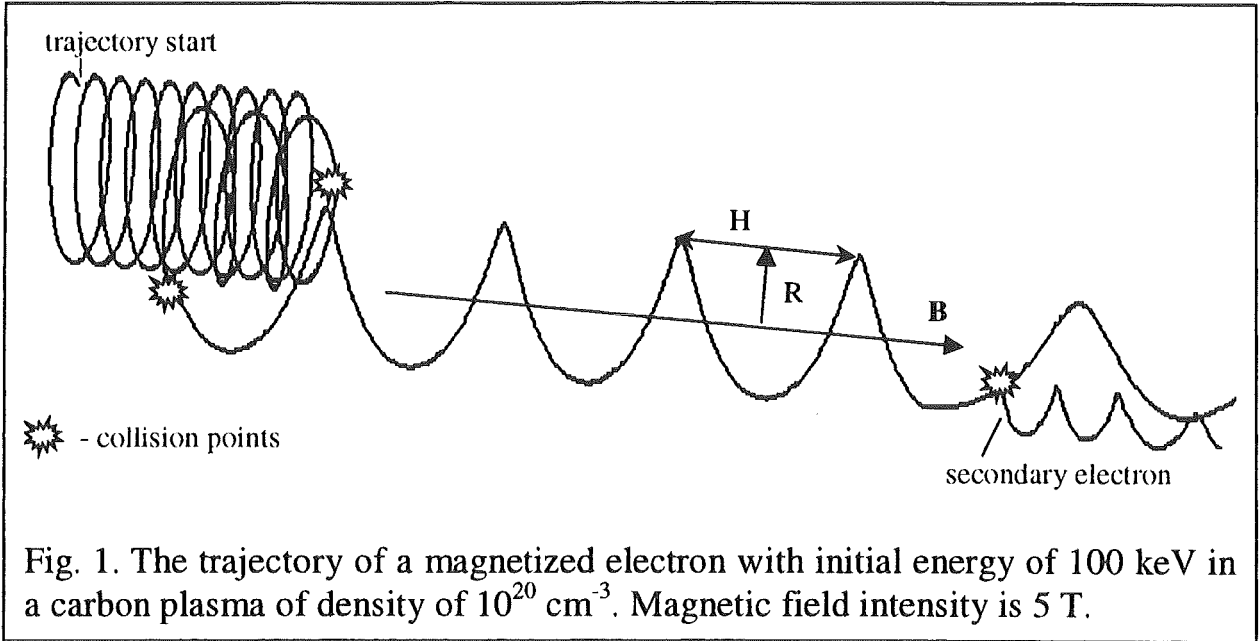
layer of inhomogeneous carbon plasma is approximately 20 μm for the case when the magnetic field lines make an angle of 5° with the plasma surface.

In conclusion, it should be noted that the Monte Carlo calculations on the energy deposition were performed for separate temporal states of the expanding carbon plasma. In reality, the self-consistent calculations of the rapidly expanding, high-energy-density plasmas and energy deposition into these plasmas by incident radiation are of special interest. It requires the coupling of energy deposition model into a time-dependent magnetohydrodynamic code. For this purpose, the developed Monte Carlo energy deposition model must retain enough generality and flexibility to remain sufficiently efficient to be used as a subprogram in the large hydrodynamic code such as FOREV-2 [2] used for studying target physics and particle transport. Thus, further development may be directed to the simplification and optimization of the energy deposition model used to save computational time and to implement it into a hydrodynamics computer code.

6. REFERENCES

1. R. Parker et al J. Nucl. Mater. 241-243 (1997) 1.
2. H Wuerz et al *Hot plasma target interaction and quantification of erosion of the ITRE slot divertor during disruptions and ELMS*. Report FZKA 6198 Forschungszentrum Karlsruhe 1999.
3. L. Eyges, *Multiple scattering with energy loss*, Phys. Rev. **74** 1534 (1948).
4. S.A. Goudsmit and Saunderson, *Multiple scattering of electrons*, Phys. Rev. **57** 24 (1940).
5. S.A. Goudsmit and Saunderson, *Multiple scattering of electrons*. II, Phys. Rev. **58** 36 (1940).
6. G. Z. Molière, *Theorie der Streuung schneller geladener Teilchen. I, Einzelstreuung am abgeschirmten Coulomb-Feld*, Z. Naturforsch **2a** 133 (1947).
7. G. Z. Molière, *Theorie der Streuung schneller geladener Teilchen. II, Mehrfach- und Vielfachstreuung*, Z. Naturforsch **3a** 78 (1948).

8. H.A. Bethe, *Molière's theory of multiple scattering*, Phys. Rev. 89 1256 (1953).
9. K.B. Winterbon, *Finite-angle multiple scattering*, Nuclear Instruments and Methods **B21** 1 (1987).
10. L. Landau, *On the energy loss of fast particles by ionization*, J. Phys. USSR, **8** 201 (1944).
11. O. Blunck and S. Leisegang, *Zum Energieverlust schneller Elektronen in dünnen Schichten*, Z. Physik **128** 500 (1950).
12. L.D. Landau and E.M. Lifshitz, *Quantum Mechanics (Non-Relativistic theory)*, Vol. 3, Pergamon Press, 1979.
13. E.J. Williams, *The straggling of β -particles*, Proc. Roy. Soc. **A125** 420 (1929).
14. H.A. Bethe, *Theory of passage of swift corpuscular rays through matter*, Ann. Physik **5** 325 (1930).
15. H.A. Bethe, *Scattering of electrons*, Z. für Physik **76** 293 (1932).
16. F. Bloch, *Stopping power of atoms with several electrons*, Z. für Physik **81** 363 (1933).
17. B.N. Bazylev, L.V. Golub, G.S. Romanov and V.I. Tolkach, *Calculation of optical physical parameters of multi-charged plasma on the base of HFS method. I. Spectral characteristics*, Journal of Engineering Physics and Thermophysics **58**, 1012 (1990).
18. B.N. Bazylev, L.V. Golub, G.S. Romanov and V.I. Tolkach, *Calculation of optical physical parameters of multi-charged plasma on the base of HFS method. II. Average and group-averaged absorption coefficients*, Journal of Engineering Physics and Thermophysics **59**, 62 (1990).
19. J.H. Hammersley and D.C. Handscomb, *Monte Carlo Methods*, Wiley & Sons Inc., New York, 1964.
20. Y.A. Shreider (Ed.), *The Monte Carlo Method*, Pergamon Press, New York, 1966.
21. J.W. Butler, *Machine Sampling from Given Probability Distributions*, from Symposium on Monte Carlo Methods, H.A. Meyer (Ed.), Wiley & Sons, New York, 1966.
22. W.A. Coleman, *Mathematical verification of a certain Monte Carlo sampling technique and applications of the technique to radiation transport problems*, Nucl. Sci. Engng **32** 76 (1968).
23. N.F. Mott and H.S.W. Massey, *The theory of atomic collisions*, Oxford, 1965.



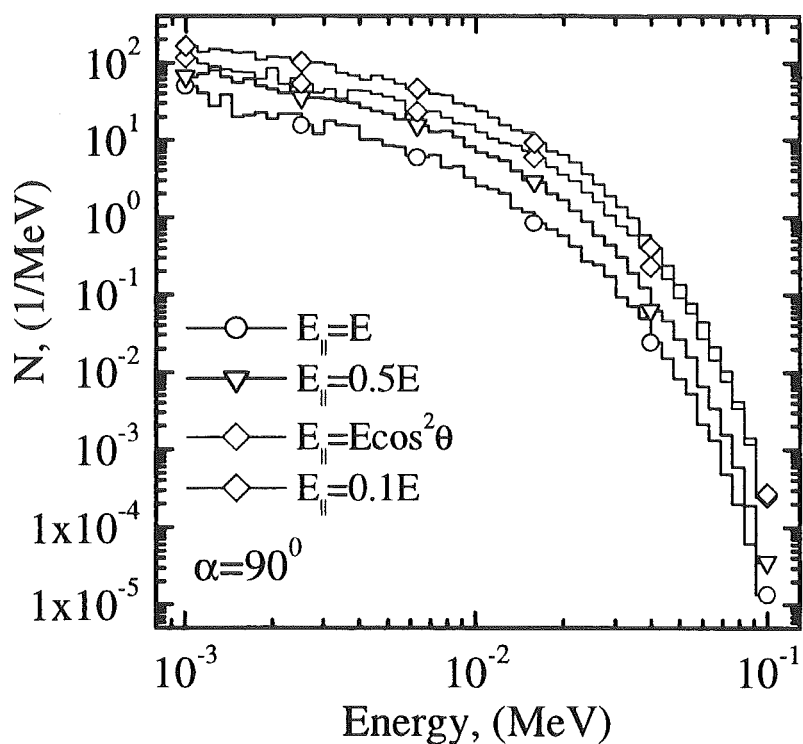


Fig. 3. Energy spectra of electrons reflected from graphite for different longitudinal energies. The magnetic lines are perpendicular to the graphite surface.

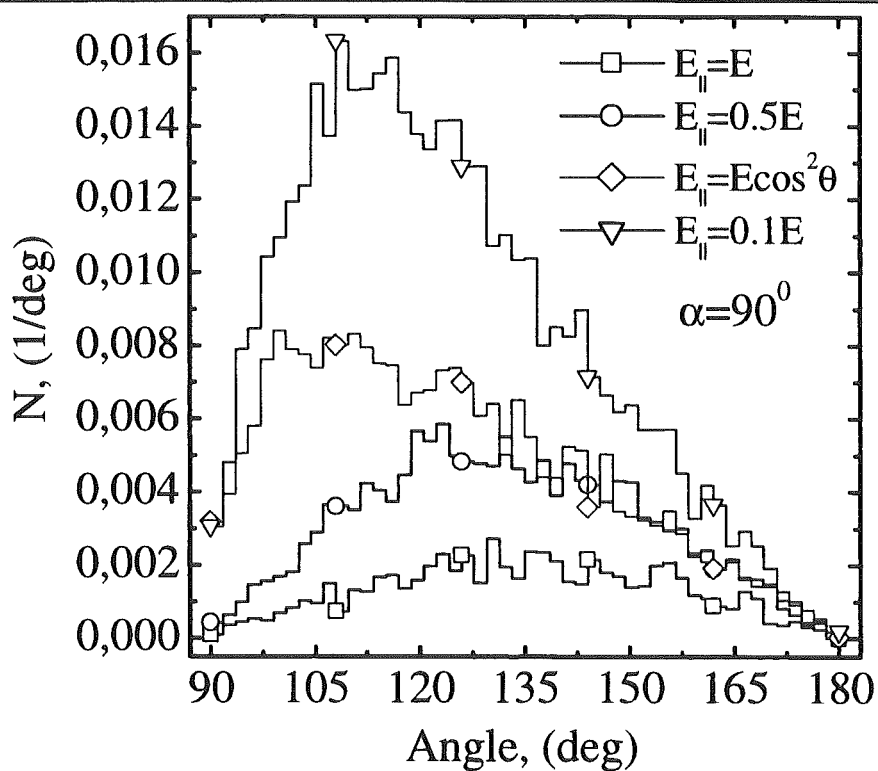


Fig. 4. Angular spectra of electrons reflected from graphite for different longitudinal energies. The magnetic lines are perpendicular to the graphite surface.

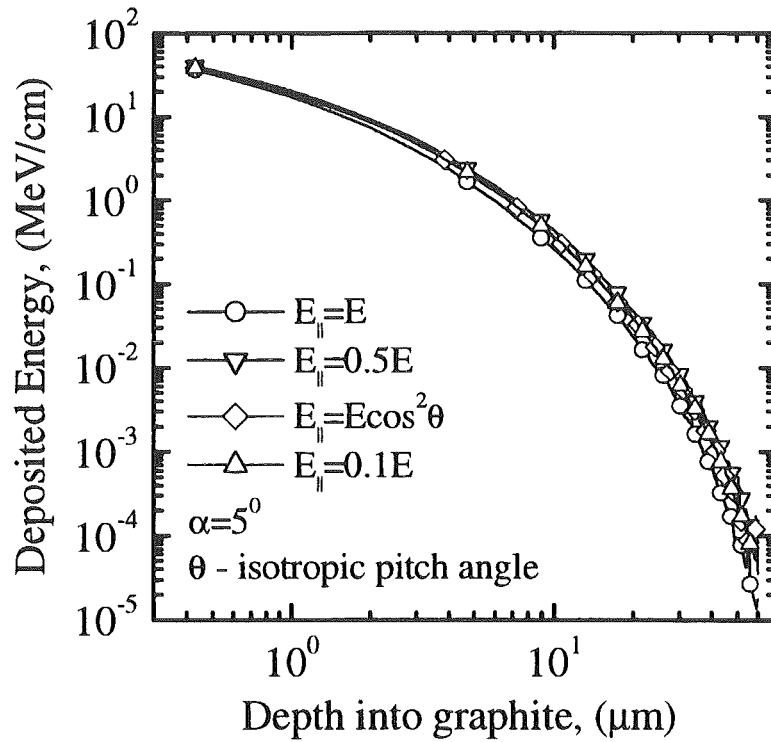


Fig. 5. Distributions of the energy deposition by Maxwellian electrons into graphite for different longitudinal energies. E - Maxwellian distributed energy of incident electrons with temperature 10 keV. E_{\parallel} - longitudinal energy of incident electrons. θ - isotropic pitch angle. α - angle formed by magnetic lines with the graphite surface.

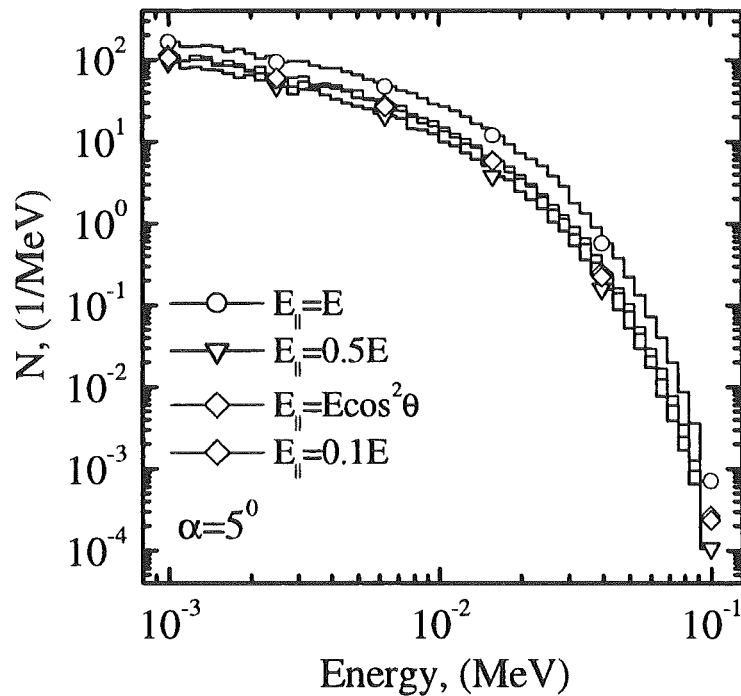


Fig. 6. Energy spectra of electrons reflected from graphite for different longitudinal energies. The magnetic lines form an angle of 5° with the graphite surface.

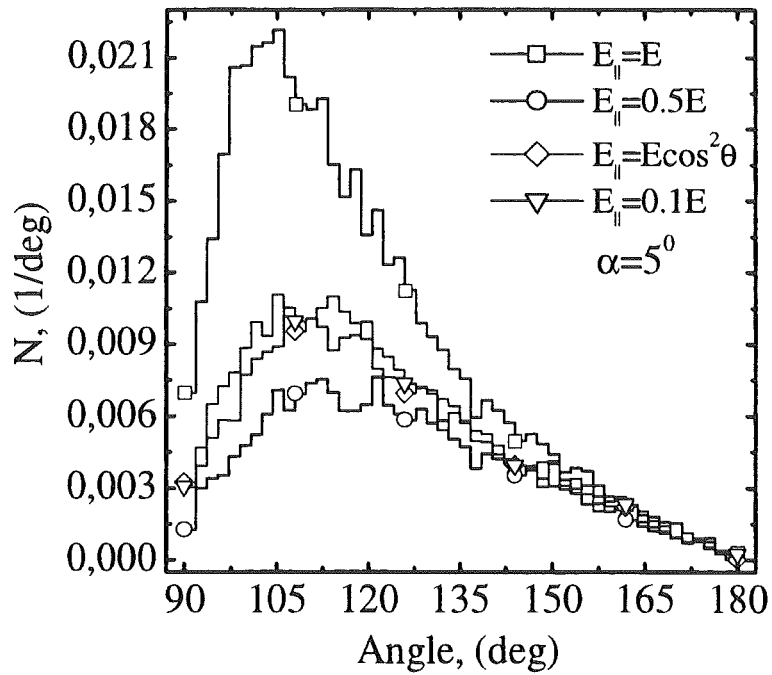


Fig. 7. Angular spectra of electrons reflected from graphite for different longitudinal energies. The magnetic lines form an angle of 5° with the graphite surface.

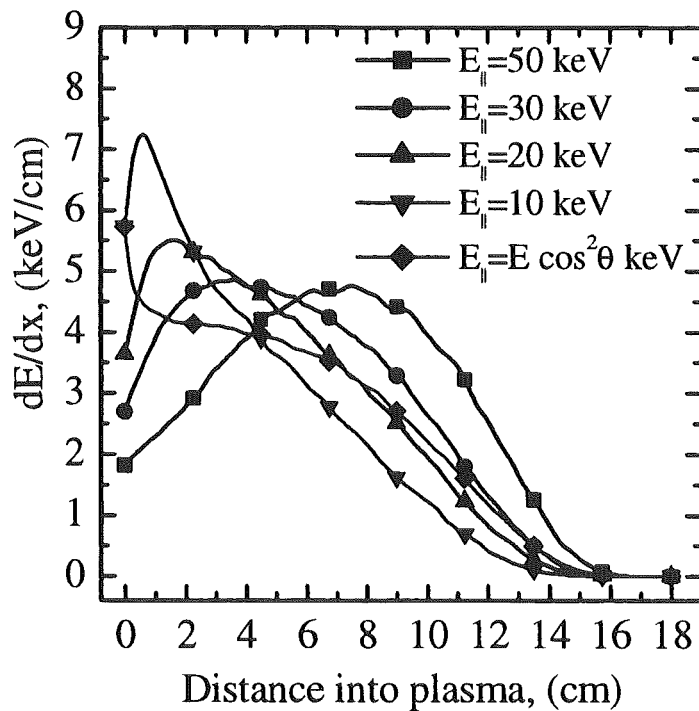


Fig. 8. Distribution of the energy deposition into a carbon plasma as a function of the longitudinal energy component E_{\parallel} . Plasma density 10^{19} cm^{-3} , plasma temperature 20 eV, monoenergetic energy $E=50 \text{ keV}$, magnetic field $B=5 \text{ T}$, angle of magnetic field lines with the plasma surface $\alpha=90^\circ$, θ - isotropic pitch angle.

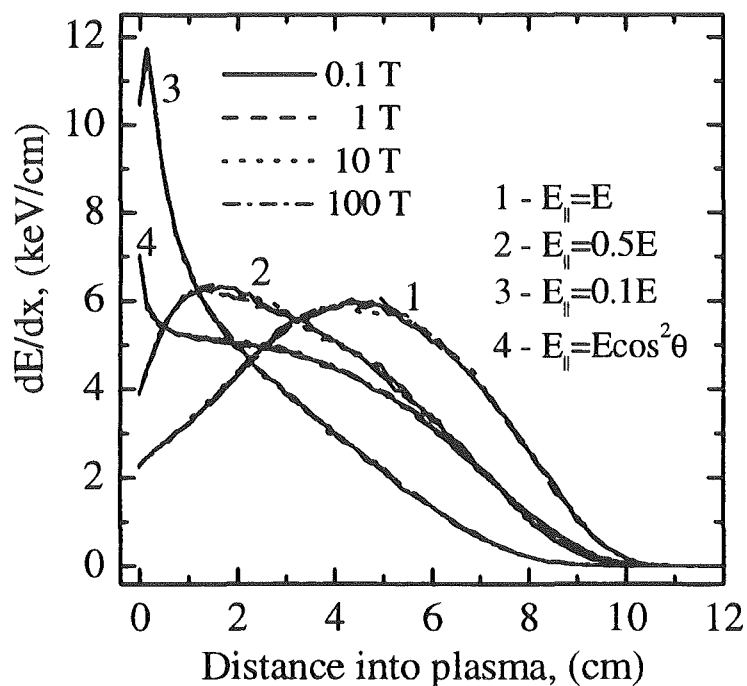


Fig. 9. Distribution of the energy deposition into a carbon plasma as function of the magnetic field intensity for different longitudinal energy components. Plasma density 10^{19} cm^{-3} , plasma temperature 20 eV, monoenergetic energy $E=40 \text{ keV}$, θ - isotropic pitch angle, angle of magnetic field lines with the plasma surface $\alpha=90^\circ$.

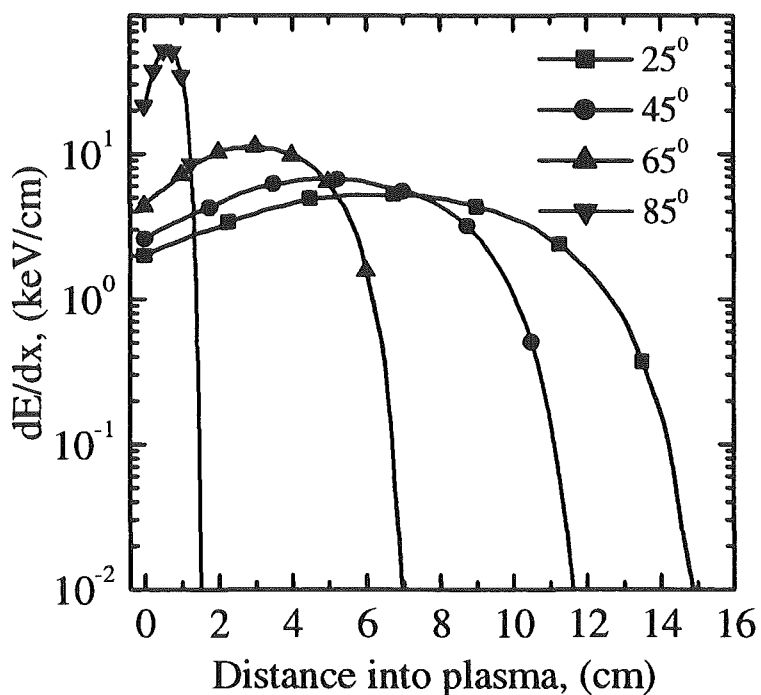


Fig. 10. Distribution of the energy deposition into the carbon plasma as a function of the incident angle. Plasma density 10^{19} cm^{-3} , plasma temperature 20 eV, monoenergetic energy $E=50 \text{ keV}$, longitudinal energy $E_{\parallel} = E$, magnetic field $B=5 \text{ T}$.

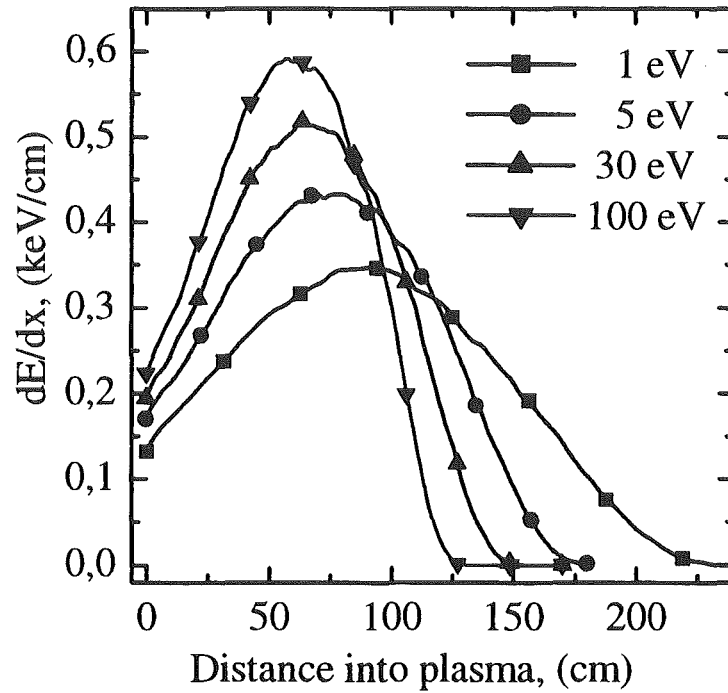


Fig. 11. Distribution of the energy deposition into the carbon plasma as a function of the plasma temperature. Plasma density 10^{18} cm^{-3} , monoenergetic energy $E=50 \text{ keV}$, longitudinal energy $E_{\parallel}=E$, magnetic field $B=5 \text{ T}$, angle of magnetic field lines with the plasma surface $\alpha=90^{\circ}$.

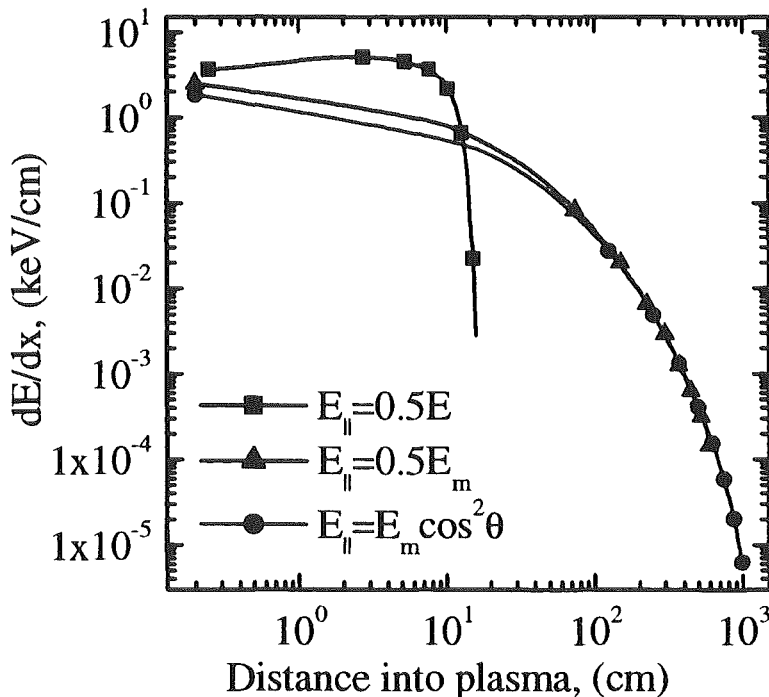


Fig. 12. Distributions of the energy deposition into the carbon plasma by monoenergetic and Maxwellian electrons. Plasma density 10^{19} cm^{-3} , plasma temperature 20 eV , monoenergetic energy $E=50 \text{ keV}$, E_m - Maxwellian distributed energy of incident electrons with temperature 50 keV , magnetic field $B=5 \text{ T}$, angle of magnetic field lines with the plasma surface $\alpha=90^{\circ}$, θ - isotropic pitch angle.

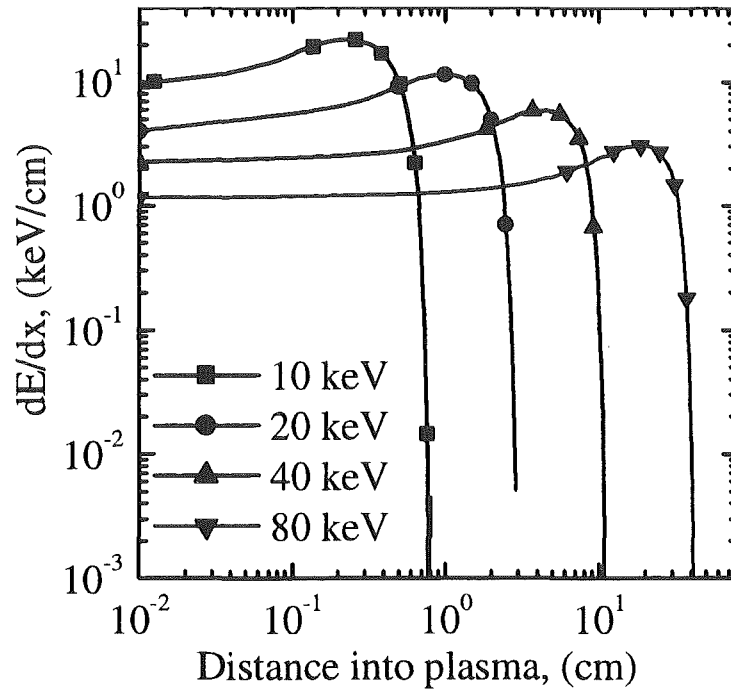


Fig. 13. Distribution of the energy deposition into the carbon plasma as a function of the monoenergetic incident energy E . Plasma density 10^{19} cm^{-3} , plasma temperature 20 eV, longitudinal energy $E_{\parallel} = E$, magnetic field $B=5 \text{ T}$, angle of magnetic field lines with the plasma surface $\alpha=90^{\circ}$.

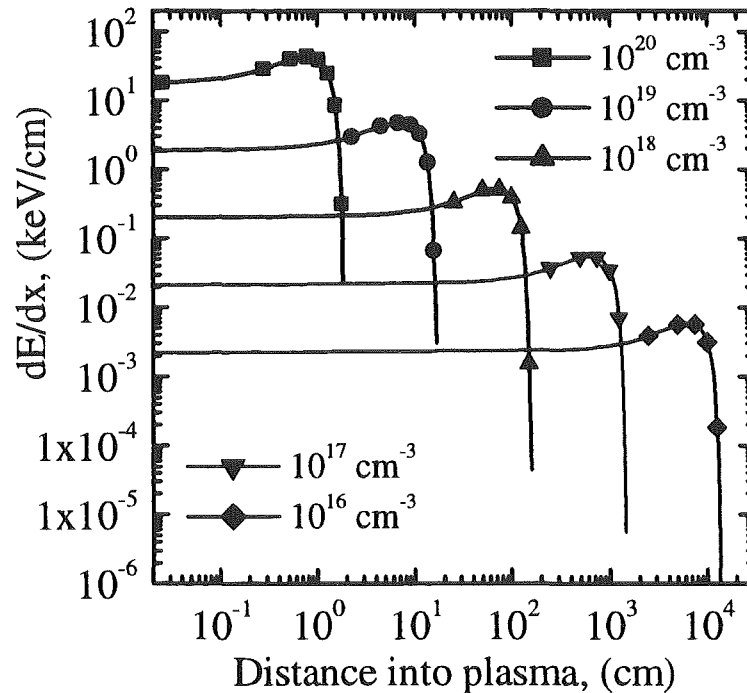


Fig. 14. Distribution of the energy deposition into the carbon plasma as a function of the plasma density. Plasma temperature 20 eV, monoenergetic energy $E=50 \text{ keV}$, longitudinal energy $E_{\parallel} = E$, magnetic field $B=5 \text{ T}$, angle of magnetic field lines with the plasma surface $\alpha=90^{\circ}$.

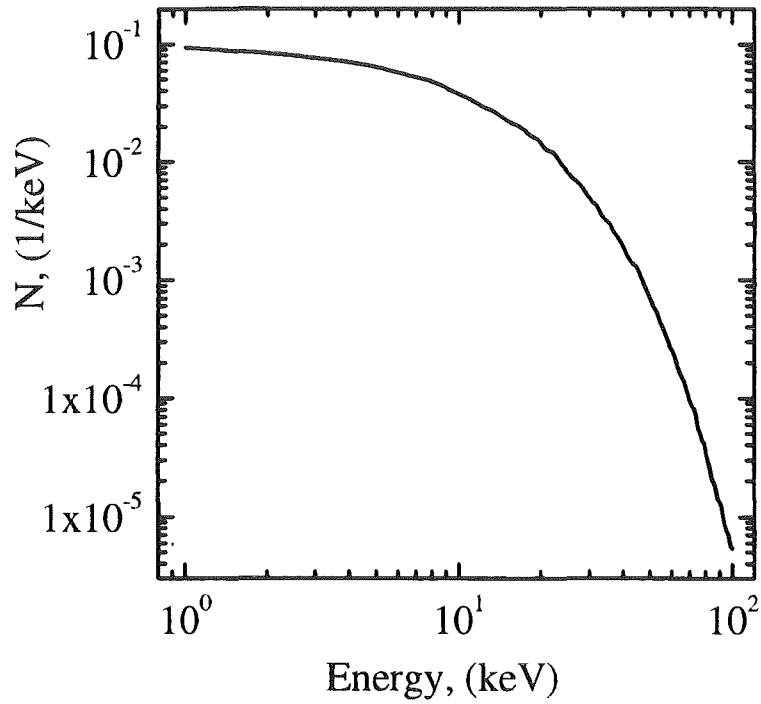


Fig. 15. Two-dimensional Maxwellian function of the energy distribution in the incident electron flux with the temperature 10 keV.

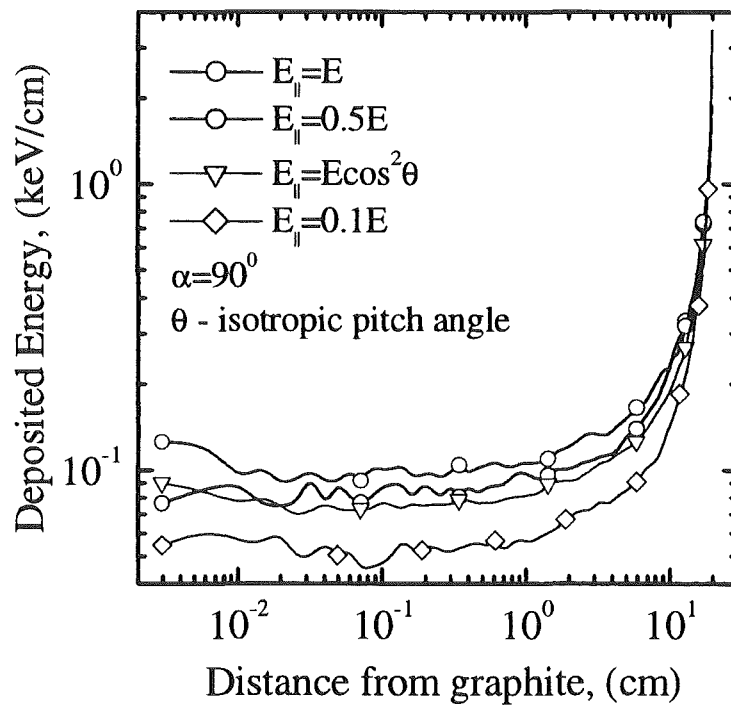


Fig. 16. Distribution of the energy deposition into the homogeneous plasma shield for different longitudinal energies. The magnetic field lines are perpendicular to the plasma surface. Plasma density 10^{18} cm^{-3} , plasma temperature 5 eV, E - Maxwellian distributed energy of incident electrons with temperature 10 keV, magnetic field $B=5 \text{ T}$, θ - isotropic pitch angle.

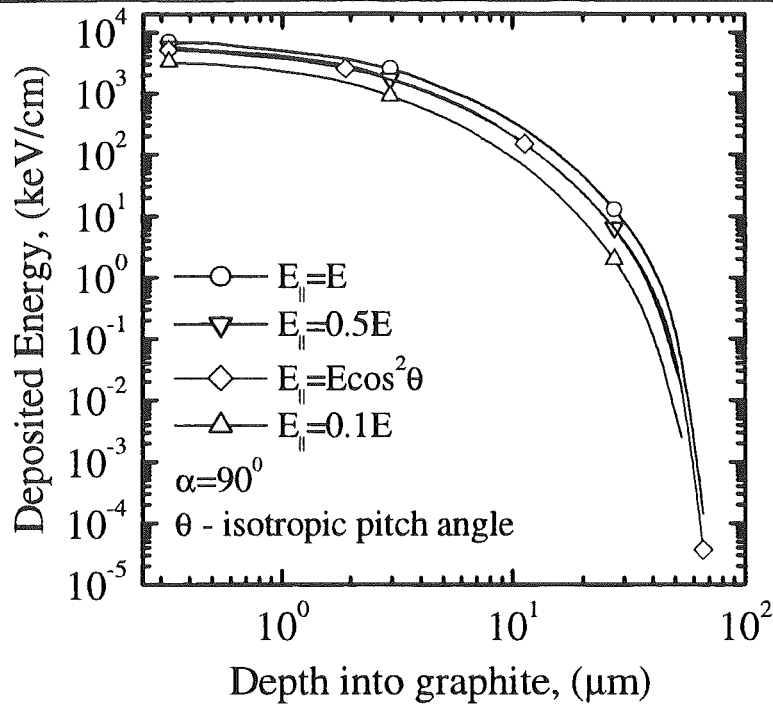


Fig. 17. Distribution of the energy deposition for different longitudinal energies into graphite shielded by a layer of homogeneous carbon plasma of the thickness of 20 cm. The magnetic field lines are perpendicular to the plasma surface. E - Maxwellian distributed energy of incident electrons with temperature 10 keV, magnetic field $B=5$ T, θ - isotropic pitch angle.

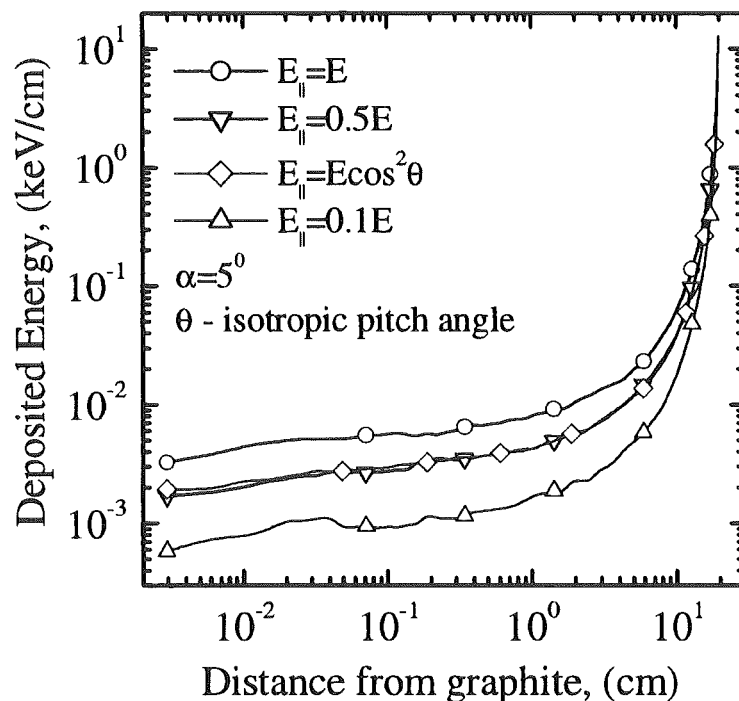


Fig. 18. Distribution of the energy deposition into the homogeneous plasma shield for different longitudinal energies. The magnetic field lines form an angle of 5° with the plasma surface. Plasma density 10^{18} cm^{-3} , plasma temperature 5 eV, E - Maxwellian distributed energy of incident electrons with temperature 10 keV, magnetic field $B=5$ T, θ - isotropic pitch angle.

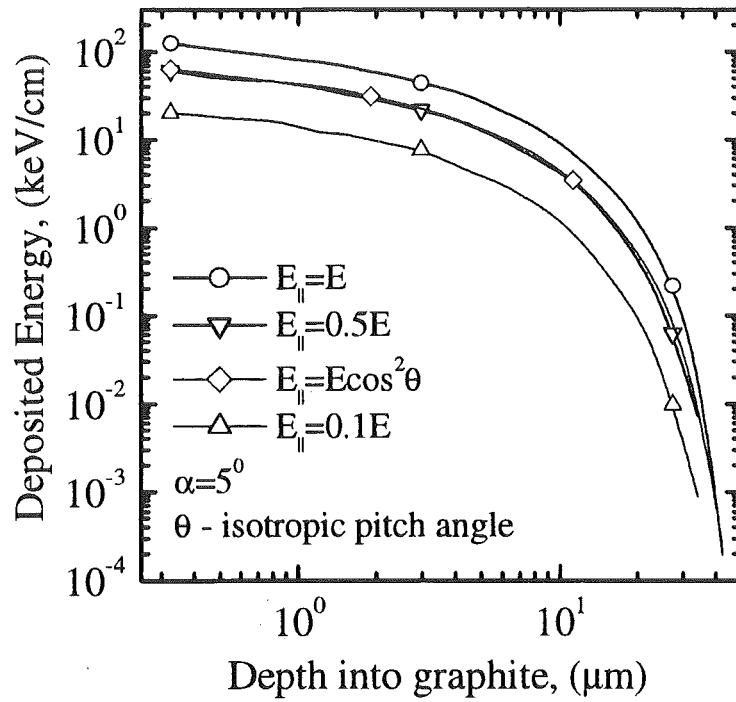


Fig. 19. Distribution of the energy deposition for different longitudinal energies into graphite shielded by a layer of homogeneous carbon plasma of the thickness of 20 cm. The magnetic field lines form an angle of 5° with the plasma surface. E - Maxwellian distributed energy of incident electrons with temperature 10 keV, magnetic field $B=5$ T, θ - isotropic pitch angle.

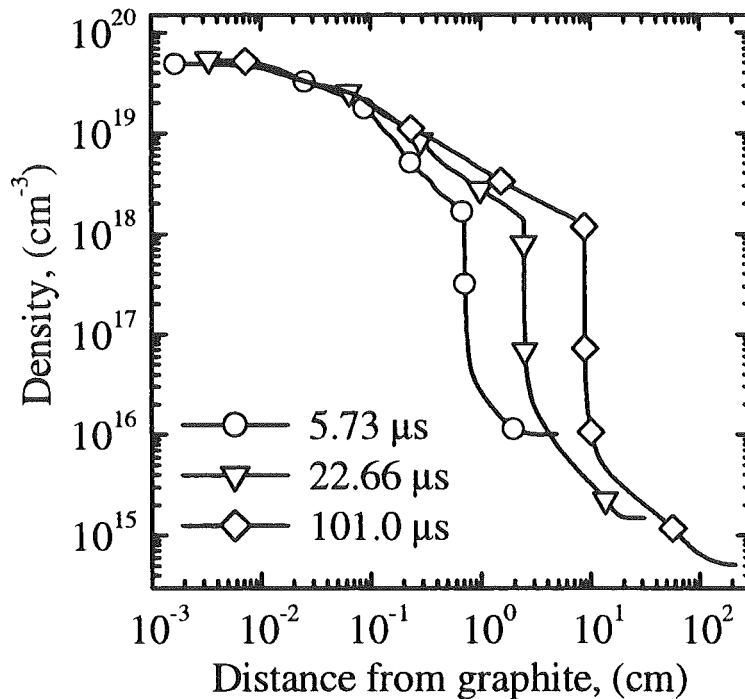


Fig. 20. Density distribution in a carbon plasma shield at 5.73, 22.66, and 101.0 μs .

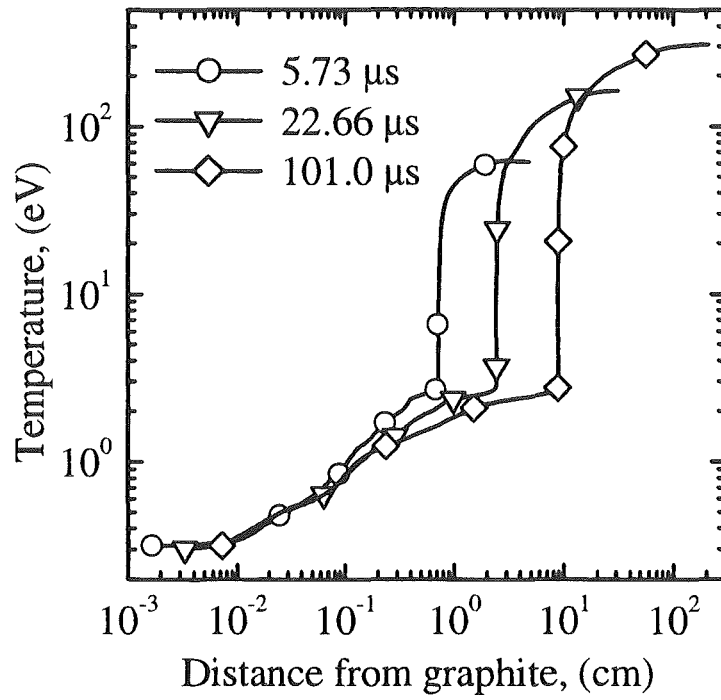


Fig. 21. Temperature distribution in a carbon plasma shield at 5.73, 22.66, and 101.0 μs .

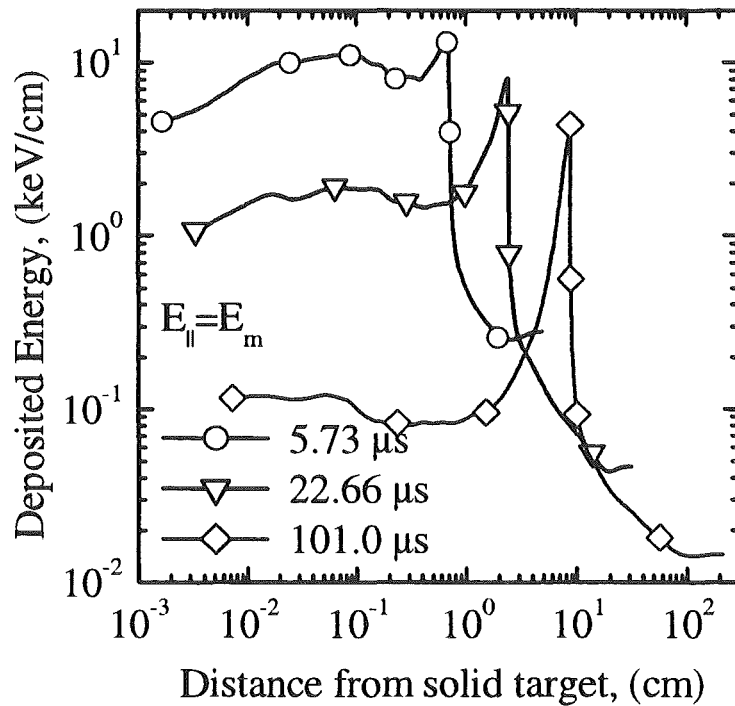


Fig. 22. Distribution of the energy deposition by the magnetized electrons with longitudinal energy $E_{||} = E_m$ into the inhomogeneous carbon plasma shield at 5.73, 22.66, and 101.0 μs . The magnetic lines form an angle of 5° with the plasma shield. E_m - Maxwellian distributed energy of the incident electrons with temperature 10 keV, magnetic field $B = 5$ T.

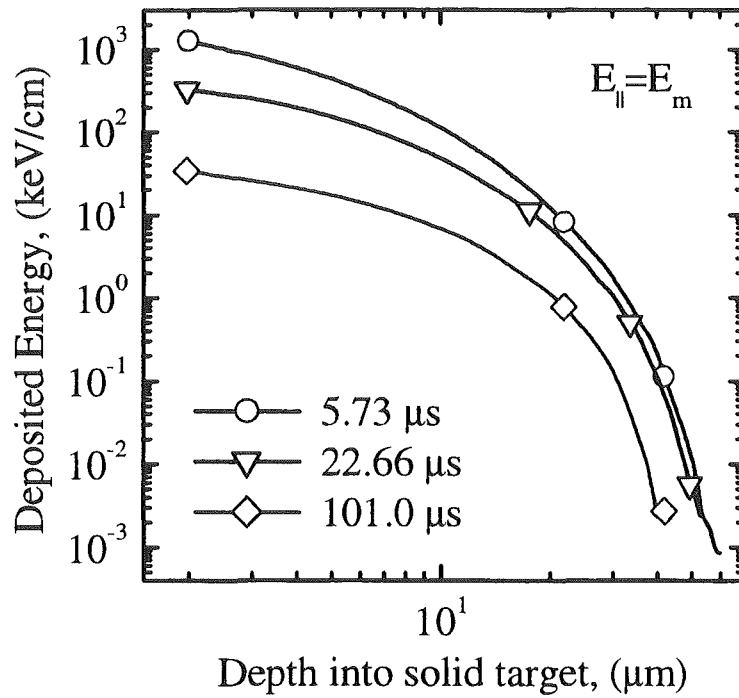


Fig. 23. Distribution of the energy deposition by the magnetized electrons with longitudinal energy $E_{\parallel} = E_m$ into graphite shielded by a layer of inhomogeneous carbon plasma at 5.73, 22.66, and 101.0 μs. E_m - Maxwellian distributed energy of the incident electrons with temperature 10 keV, magnetic field $B = 5$ T.

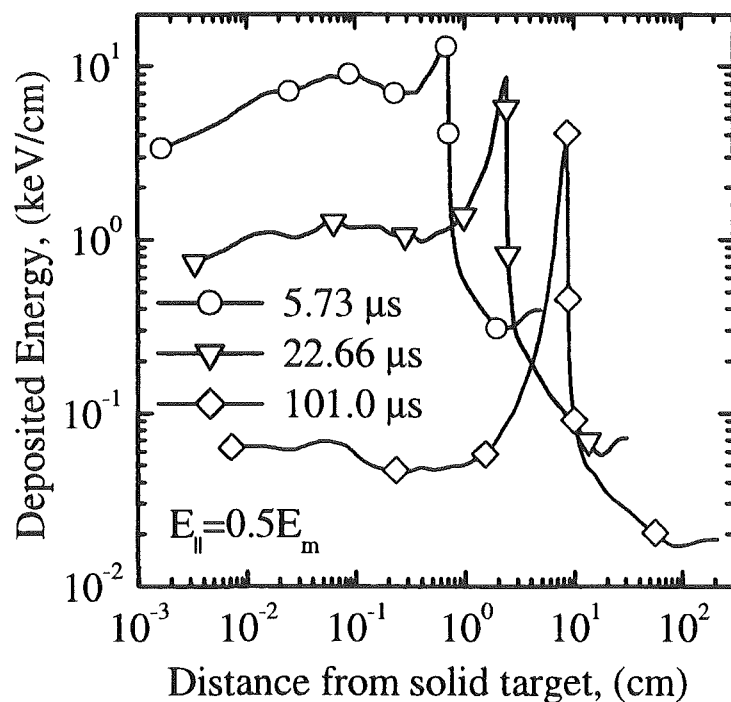


Fig. 24. Distribution of the energy deposition by the magnetized electrons with longitudinal energy $E_{\parallel} = 0.5E_m$ into the inhomogeneous carbon plasma shield at 5.73, 22.66, and 101.0 μs. The magnetic lines form an angle of 5° with the plasma shield. E_m - Maxwellian distributed energy of the incident electrons with temperature 10 keV, magnetic field $B = 5$ T.

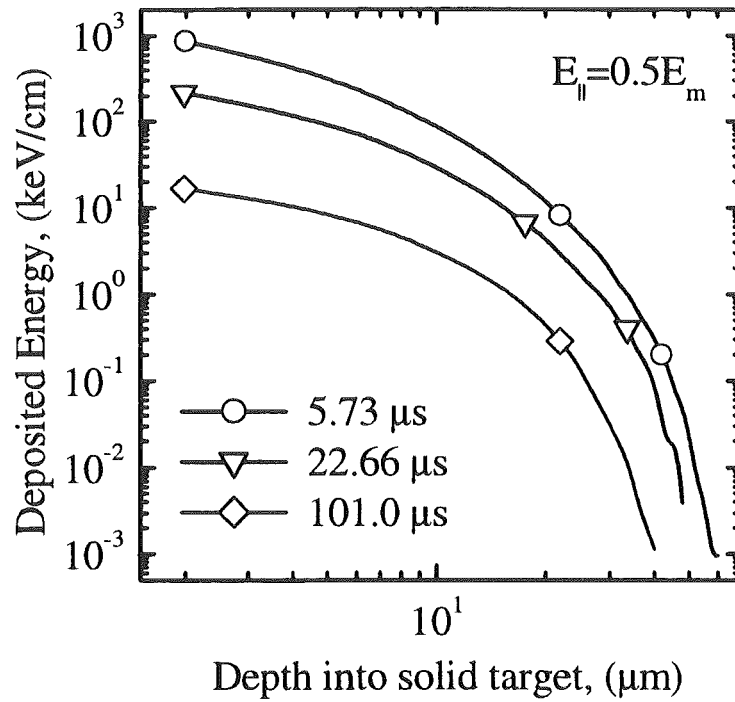


Fig. 25. Distribution of the energy deposition by the magnetized electrons with longitudinal energy $E_{||}=0.5E_m$ into graphite shielded by a layer of inhomogeneous carbon plasma at 5.73, 22.66, and 101.0 μ s. E_m - Maxwellian distributed energy of the incident electrons with temperature 10 keV, magnetic field $B=5$ T.

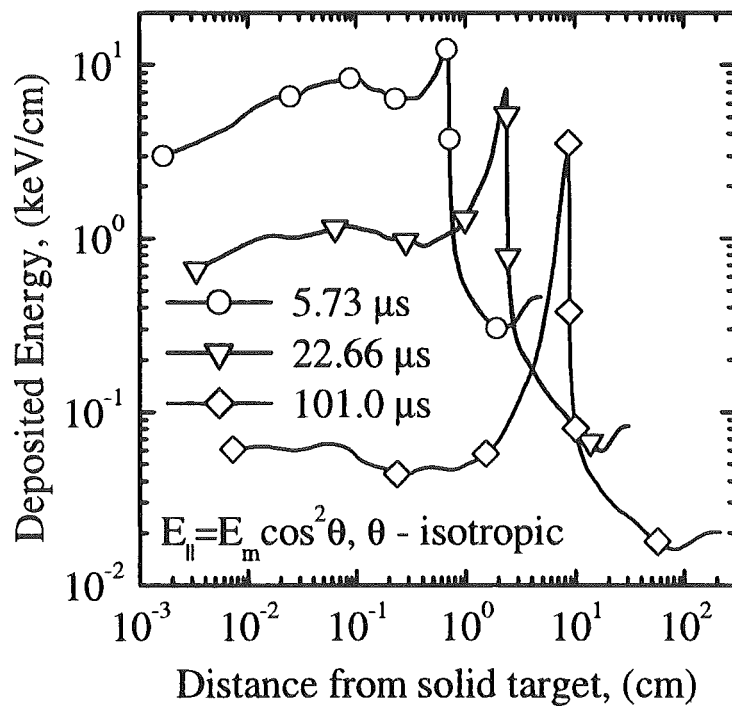


Fig. 26. Distribution of the energy deposition by the magnetized electrons with longitudinal energy $E_{||}=E_m \cos^2 \theta$ into the inhomogeneous carbon plasma shield at 5.73, 22.66, and 101.0 μ s. The magnetic lines form an angle of 5° with the plasma shield. E_m - Maxwellian distributed energy of the incident electrons with temperature 10 keV, magnetic field $B=5$ T, θ - isotropic pitch angle.

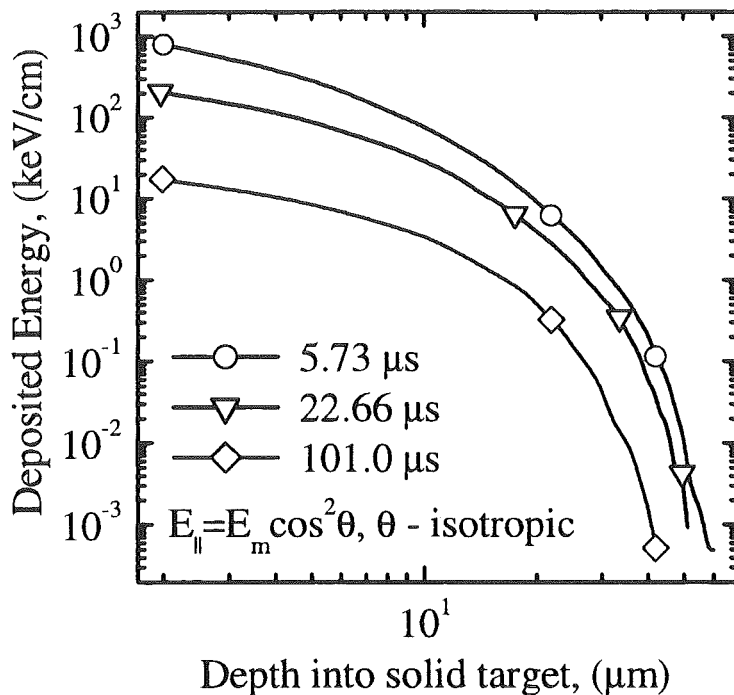


Fig. 27. Distribution of the energy deposition by the magnetized electrons with longitudinal energy $E_{\parallel} = E_m \cos^2 \theta$ into graphite shielded by a layer of inhomogeneous carbon plasma at 5.73, 22.66, and 101.0 μs . E_m - Maxwellian distributed energy of the incident electrons with temperature 10 keV, magnetic field $B = 5$ T, θ - isotropic pitch angle.

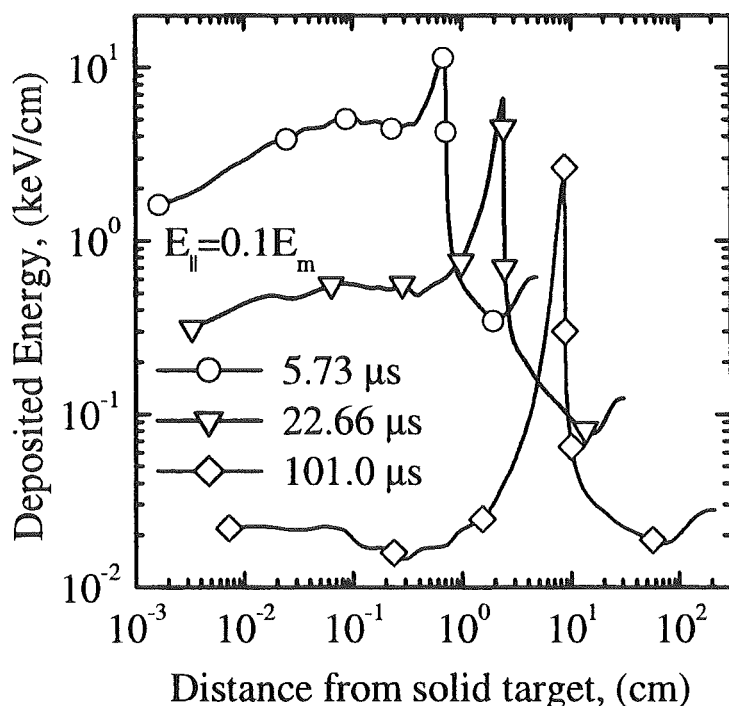


Fig. 28. Distribution of the energy deposition by the magnetized electrons with longitudinal energy $E_{\parallel} = 0.1 E_m$ into the inhomogeneous carbon plasma shield at 5.73, 22.66, and 101.0 μs . The magnetic lines form an angle of 5° with the plasma shield. E_m - Maxwellian distributed energy of the incident electrons with temperature 10 keV, magnetic field $B = 5$ T.

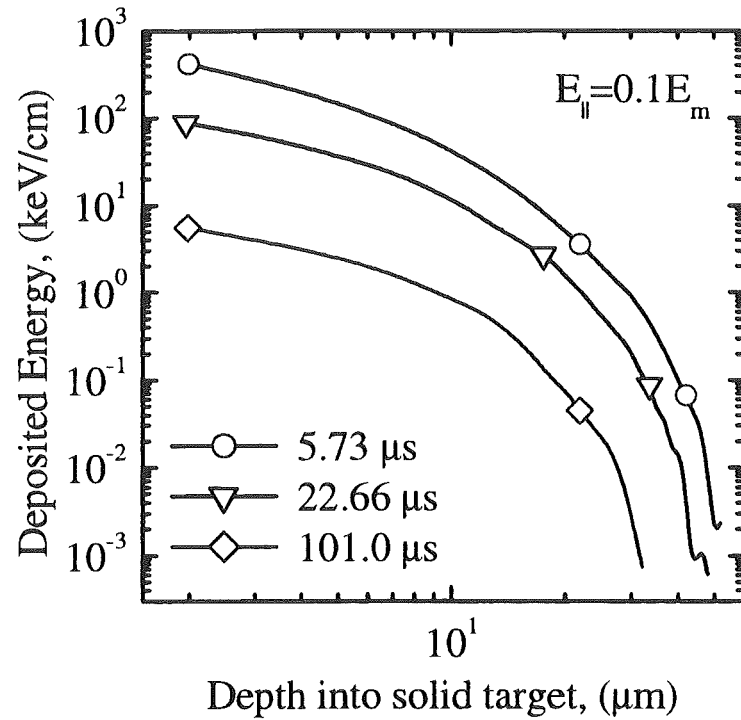


Fig. 29. Distribution of the energy deposition by the magnetized electrons with longitudinal energy $E_{||}=0.1E_m$ into graphite shielded by a layer of inhomogeneous carbon plasma at 5.73, 22.66, and 101.0 μs . E_m - Maxwellian distributed energy of the incident electrons with temperature 10 keV, magnetic field $B=5$ T.

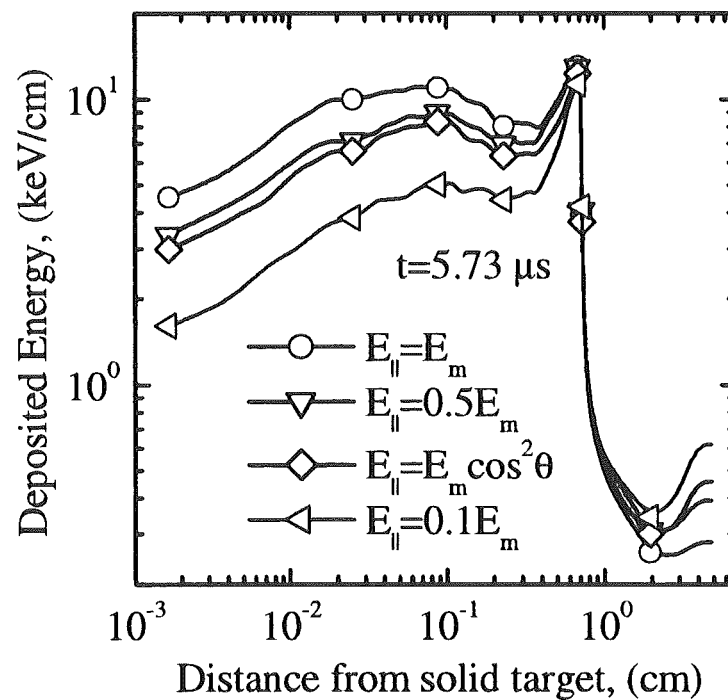


Fig. 30. Distribution of the energy deposition by the magnetized electrons with different longitudinal energies into the inhomogeneous carbon plasma shield at 5.73 μs . The magnetic lines form an angle of 5° with the plasma shield. E_m - Maxwellian distributed energy of the incident electrons with temperature 10 keV, magnetic field $B=5$ T, θ - isotropic pitch angle.

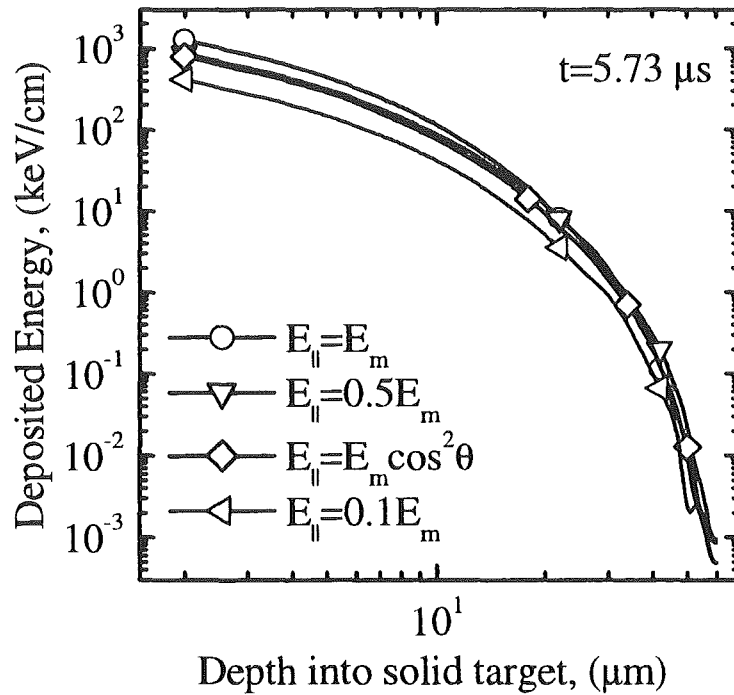


Fig. 31. Distribution of the energy deposition by the magnetized electrons with different longitudinal energies into graphite shielded by a layer of inhomogeneous carbon plasma at $5.73 \mu\text{s}$. E_m - Maxwellian distributed energy of the incident electrons with temperature 10 keV, magnetic field $B=5 \text{ T}$, θ - isotropic pitch angle.

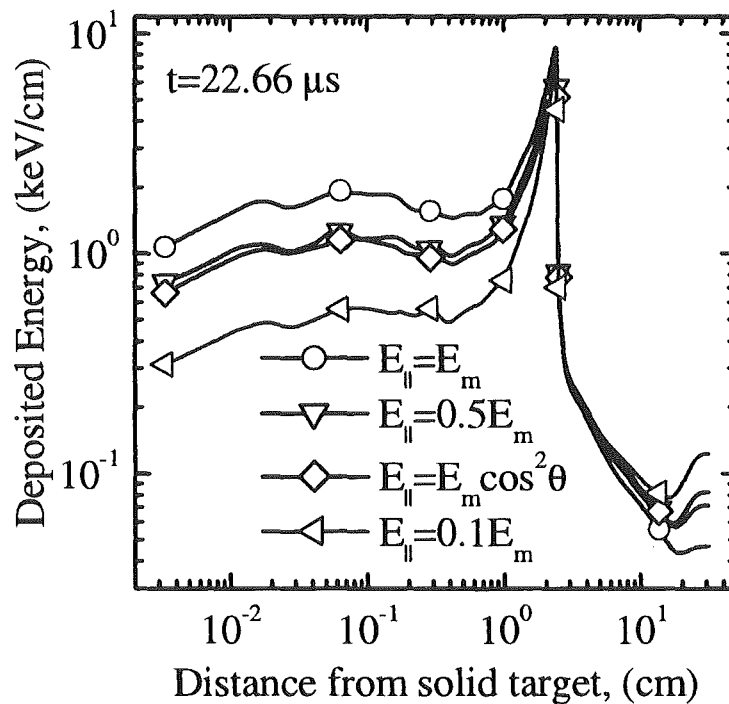


Fig. 32. Distribution of the energy deposition by the magnetized electrons with different longitudinal energies into the inhomogeneous carbon plasma shield at $22.66 \mu\text{s}$. The magnetic lines form an angle of 5° with the plasma shield. E_m - Maxwellian distributed energy of the incident electrons with temperature 10 keV, magnetic field $B=5 \text{ T}$, θ - isotropic pitch angle.

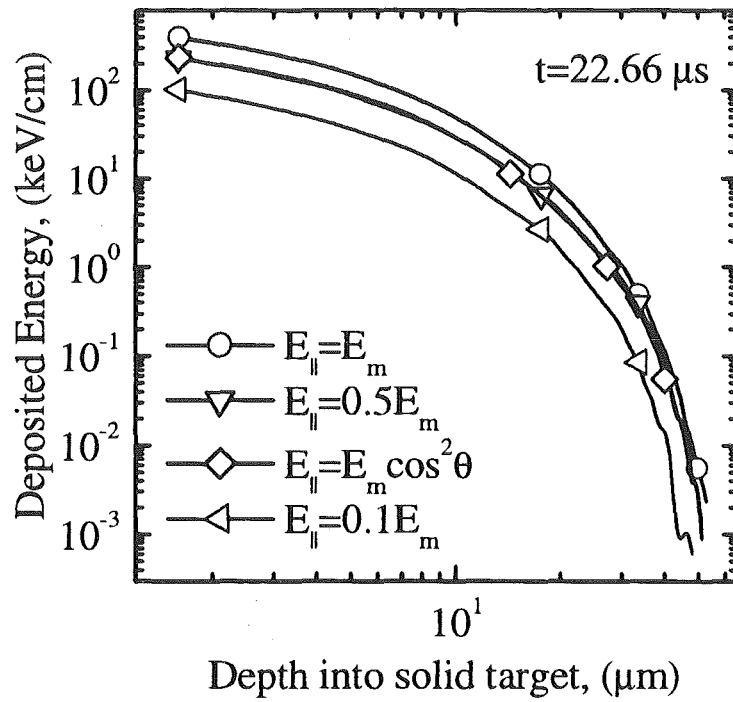


Fig. 33. Distribution of the energy deposition by the magnetized electrons with different longitudinal energies into graphite shielded by a layer of inhomogeneous carbon plasma at 22.66 μ s. E_m - Maxwellian distributed energy of the incident electrons with temperature 10 keV, magnetic field $B=5$ T, θ - isotropic pitch angle.

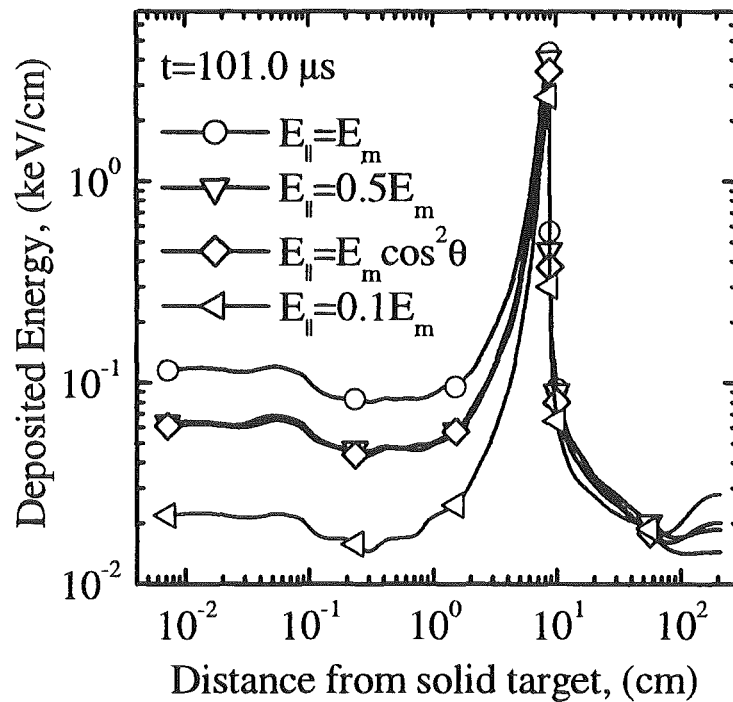


Fig. 34. Distribution of the energy deposition by the magnetized electrons with different longitudinal energies into the inhomogeneous carbon plasma shield at 101.0 μ s. The magnetic lines form an angle of 5° with the plasma shield. E_m - Maxwellian distributed energy of the incident electrons with temperature 10 keV, magnetic field $B=5$ T, θ - isotropic pitch angle.

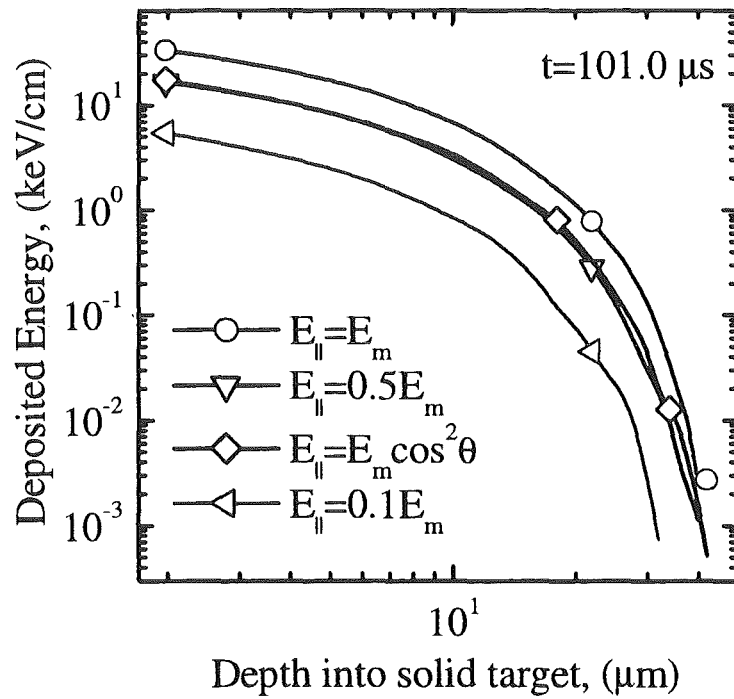


Fig. 35. Distribution of the energy deposition by the magnetized electrons with different longitudinal energies into graphite shielded by a layer of inhomogeneous carbon plasma at 101.0 μ s. E_m - Maxwellian distributed energy of the incident electrons with temperature 10 keV, magnetic field $B=5$ T, θ - isotropic pitch angle.

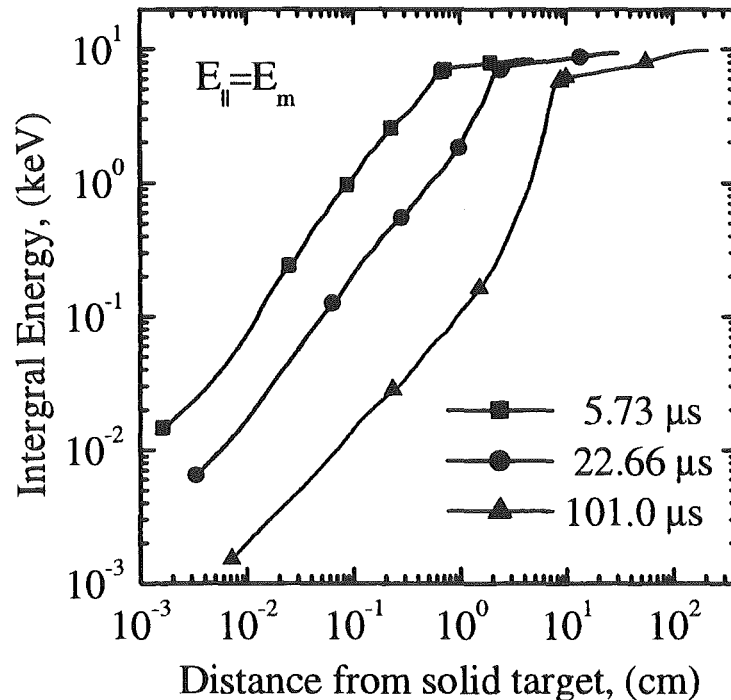


Fig. 36. Distribution of the integrated energy deposited by the magnetized electrons with the longitudinal energy $E_{||}=E_m$ into the carbon plasma shield at 5.73, 22.66, and 101.0 μ s. E_m - Maxwellian distributed energy of the incident electrons with temperature 10 keV, magnetic field $B=5$ T.

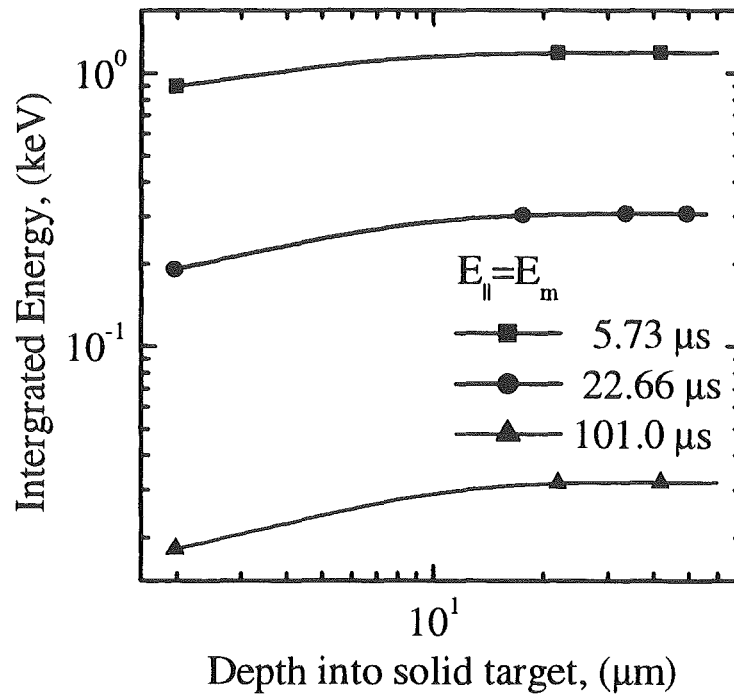


Fig. 37. Distribution of the integrated energy deposited by the magnetized electrons with the longitudinal energy $E_{||}=E_m$ into graphite shielded by a layer of inhomogeneous carbon plasma at 5.73, 22.66, and 101.0 μs . E_m - Maxwellian distributed energy of the incident electrons with temperature 10 keV, magnetic field $B=5$ T.

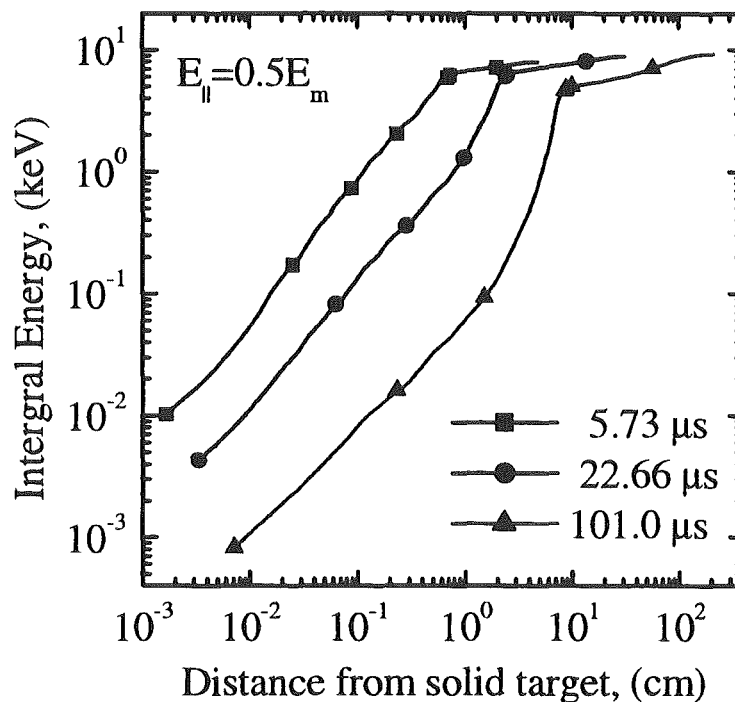


Fig. 38. Distribution of the integrated energy deposited by the magnetized electrons with the longitudinal energy $E_{||}=0.5E_m$ into the carbon plasma shield at 5.73, 22.66, and 101.0 μs . E_m - Maxwellian distributed energy of the incident electrons with temperature 10 keV, magnetic field $B=5$ T.

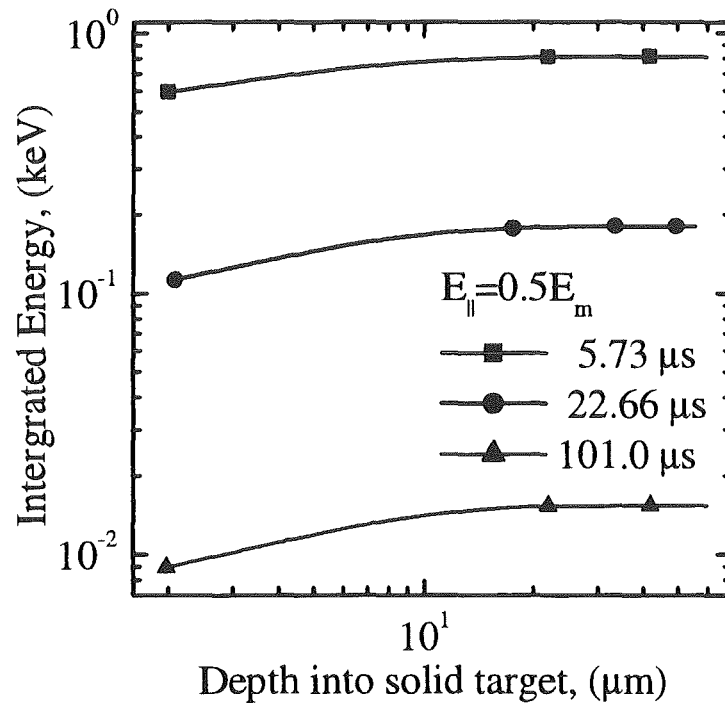


Fig. 39. Distribution of the integrated energy deposited by the magnetized electrons with the longitudinal energy $E_{\parallel} = 0.5 E_m$ into graphite shielded by a layer of inhomogeneous carbon plasma at 5.73, 22.66, and 101.0 μs . E_m - Maxwellian distributed energy of the incident electrons with temperature 10 keV, magnetic field $B = 5$ T.

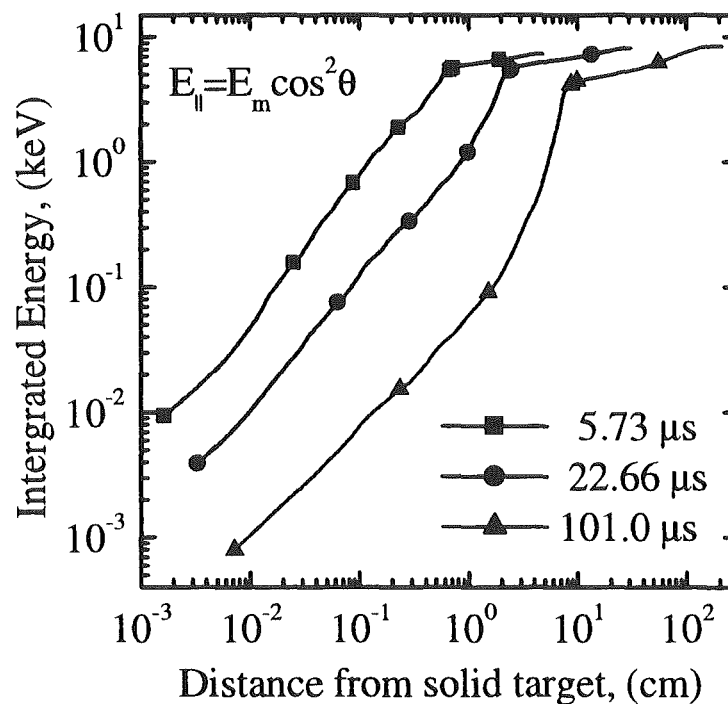


Fig. 40. Distribution of the integrated energy deposited by the magnetized electrons with the longitudinal energy $E_{\parallel} = E_m \cos^2 \theta$ into the carbon plasma shield at 5.73, 22.66, and 101.0 μs . E_m - Maxwellian distributed energy of the incident electrons with temperature 10 keV, magnetic field $B = 5$ T, θ - isotropic pitch angle.

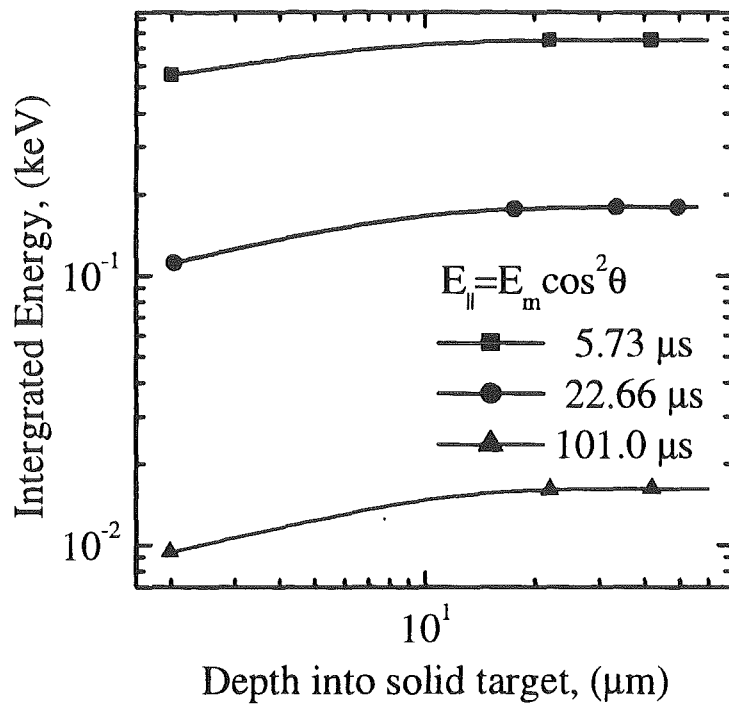


Fig. 41. Distribution of the integrated energy deposited by the magnetized electrons with the longitudinal energy $E_{\parallel} = E_m \cos^2 \theta$ into graphite shielded by a layer of inhomogeneous carbon plasma at 5.73, 22.66, and 101.0 μs . E_m - Maxwellian distributed energy of the incident electrons with temperature 10 keV, magnetic field $B = 5$ T, θ - isotropic pitch angle.

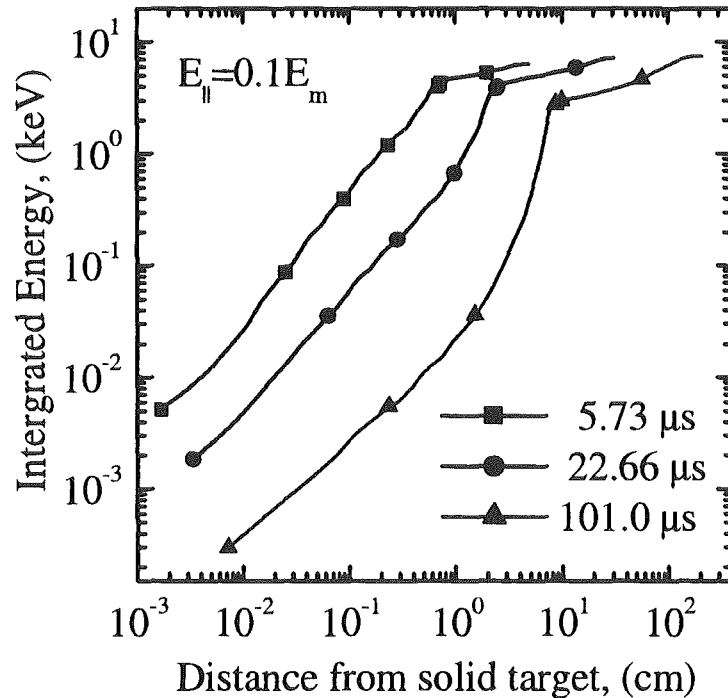


Fig. 42. Distribution of the integrated energy deposited by the magnetized electrons with the longitudinal energy $E_{\parallel} = 0.1 E_m$ into the carbon plasma shield at 5.73, 22.66, and 101.0 μs . E_m - Maxwellian distributed energy of the incident electrons with temperature 10 keV, magnetic field $B = 5$ T.

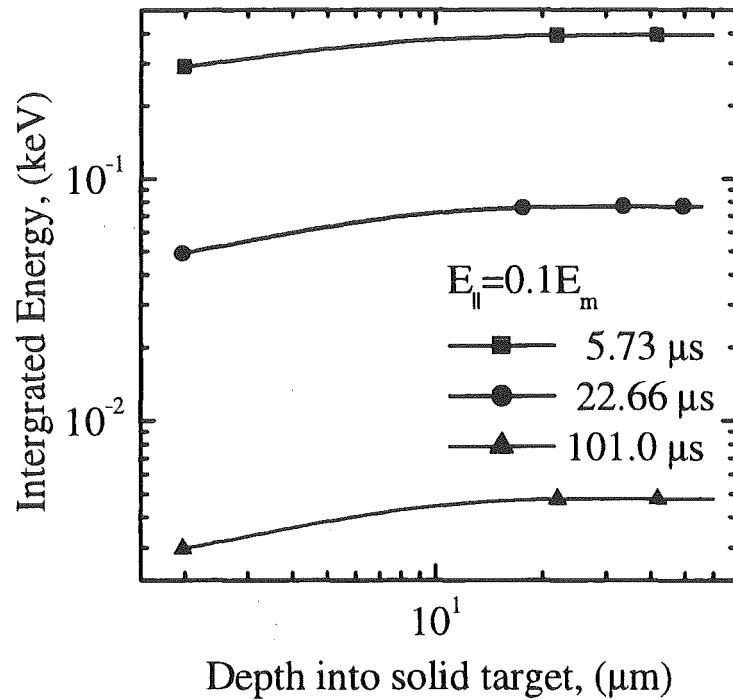


Fig. 43. Distribution of the integrated energy deposited by the magnetized electrons with the longitudinal energy $E_{||} = 0.1 E_m$ into graphite shielded by a layer of inhomogeneous carbon plasma at 5.73, 22.66, and 101.0 μs . E_m - Maxwellian distributed energy of the incident electrons with temperature 10 keV, magnetic field $B = 5$ T.

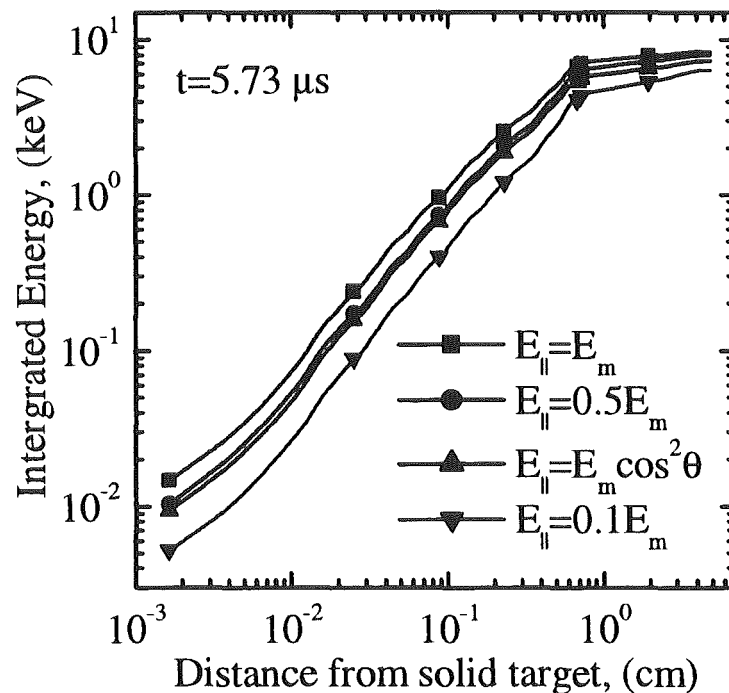


Fig. 44. Distribution of the integrated energy deposited by the magnetized electrons with different longitudinal energies into the carbon plasma shield at 5.73 μs . E_m - Maxwellian distributed energy of the incident electrons with temperature 10 keV, magnetic field $B = 5$ T, θ - isotropic pitch angle.

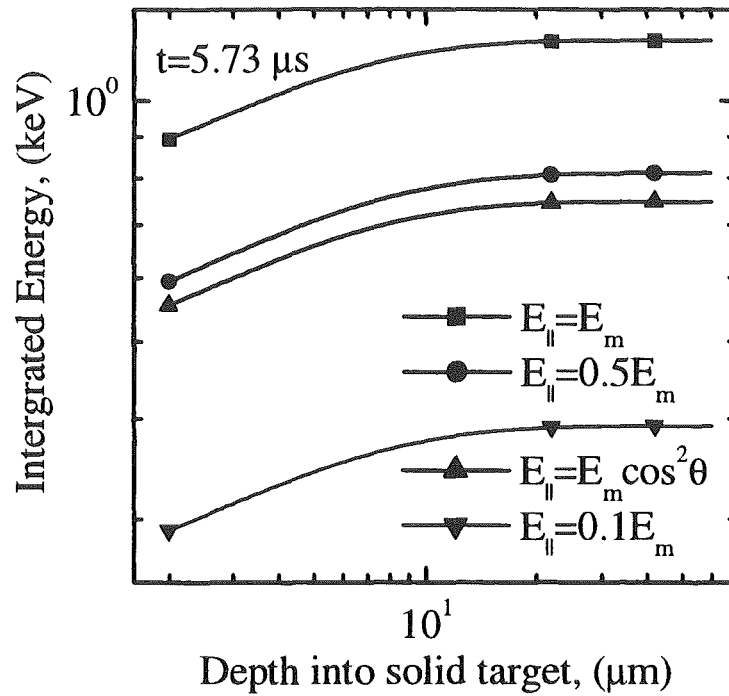


Fig. 45. Distribution of the integrated energy deposited by the magnetized electrons with different longitudinal energies into graphite shielded by a layer of inhomogeneous carbon plasma at 5.73 μs . E_m - Maxwellian distributed energy of the incident electrons with temperature 10 keV, magnetic field $B=5$ T, θ - isotropic pitch angle.

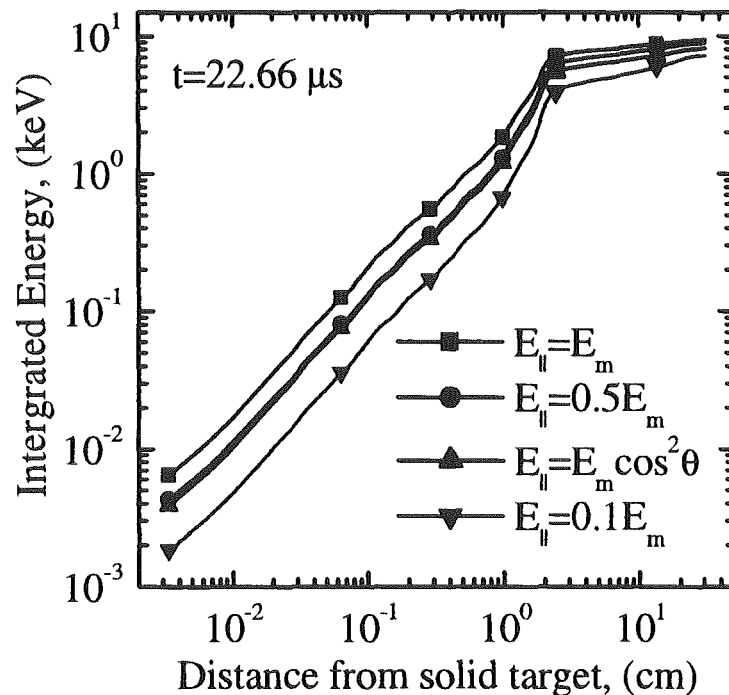


Fig. 46. Distribution of the integrated energy deposited by the magnetized electrons with different longitudinal energies into the carbon plasma shield at 22.66 μs . E_m - Maxwellian distributed energy of the incident electrons with temperature 10 keV, magnetic field $B=5$ T, θ - isotropic pitch angle.

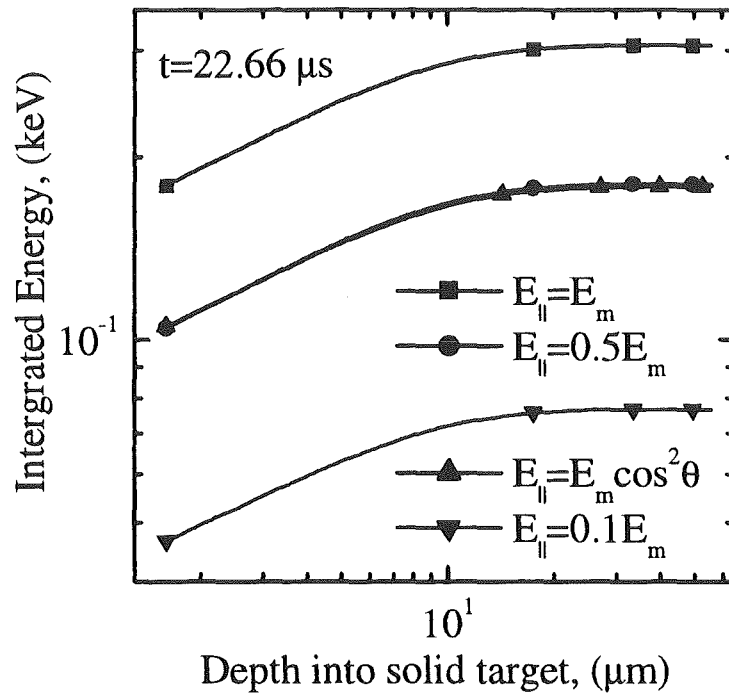


Fig. 47. Distribution of the integrated energy deposited by the magnetized electrons with different longitudinal energies into graphite shielded by a layer of inhomogeneous carbon plasma at 22.66 μs . E_m - Maxwellian distributed energy of the incident electrons with temperature 10 keV, magnetic field $B=5$ T, θ - isotropic pitch angle.

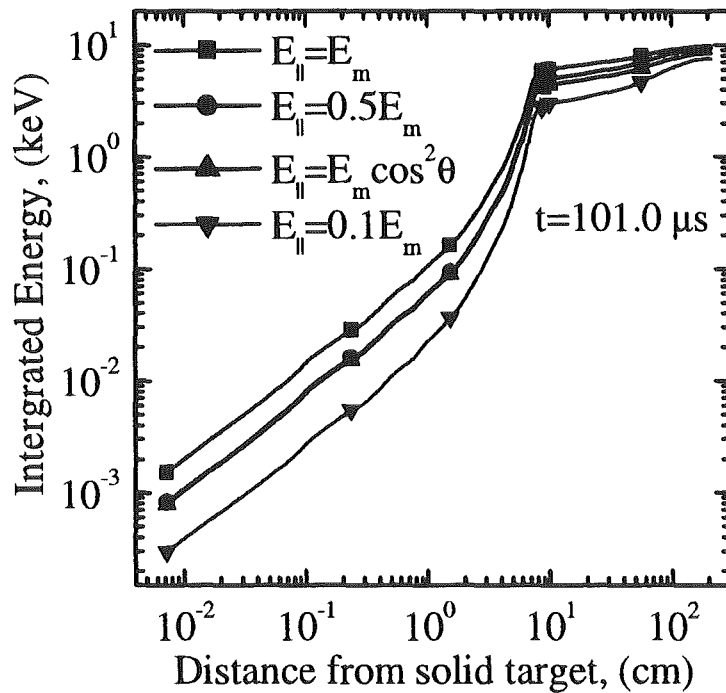


Fig. 48. Distribution of the integrated energy deposited by the magnetized electrons with different longitudinal energies into the carbon plasma shield at 101.0 μs . E_m - Maxwellian distributed energy of the incident electrons with temperature 10 keV, magnetic field $B=5$ T, θ - isotropic pitch angle.

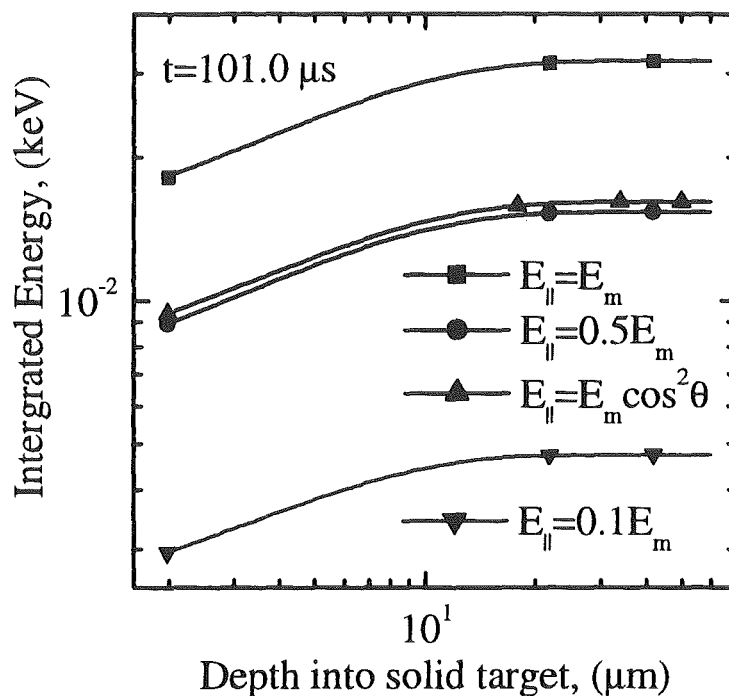


Fig. 49. Distribution of the integrated energy deposited by the magnetized electrons with different longitudinal energies into graphite shielded by a layer of inhomogeneous carbon plasma at 101.0 μs . E_m - Maxwellian distributed energy of the incident electrons with temperature 10 keV, magnetic field $B=5$ T, θ - isotropic pitch angle.

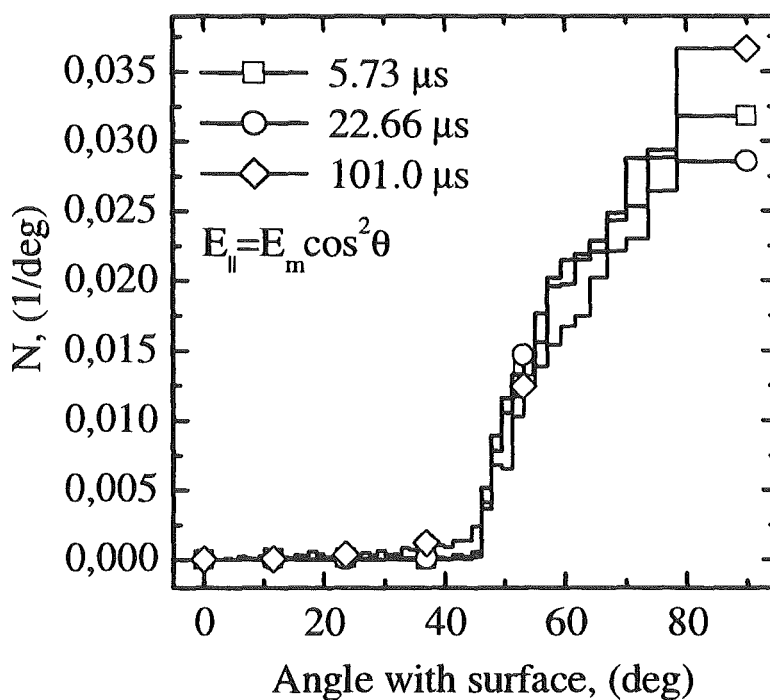


Fig. 50. Angular spectra of the Maxwellian distributed electrons with the longitudinal energy $E_{||}=E_m \cos^2 \theta$ transmitted through the inhomogeneous plasma shield and impacting onto the graphite surface. E_m - Maxwellian distributed energy of the incident electrons with temperature 10 keV, magnetic field $B=5$ T, θ - isotropic pitch angle.

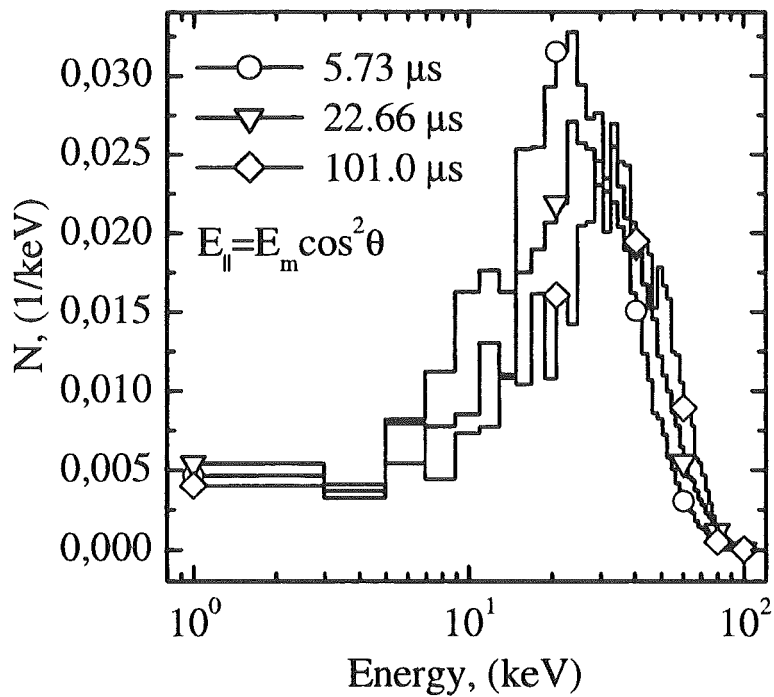


Fig. 51. Energy spectra of the Maxwellian distributed electrons with the longitudinal energy $E_{\parallel} = E_m \cos^2 \theta$ transmitted through the inhomogeneous plasma shield and impacting onto the graphite surface. E_m - Maxwellian distributed energy of the incident electrons with temperature 10 keV, magnetic field $B = 5$ T, θ - isotropic pitch angle.

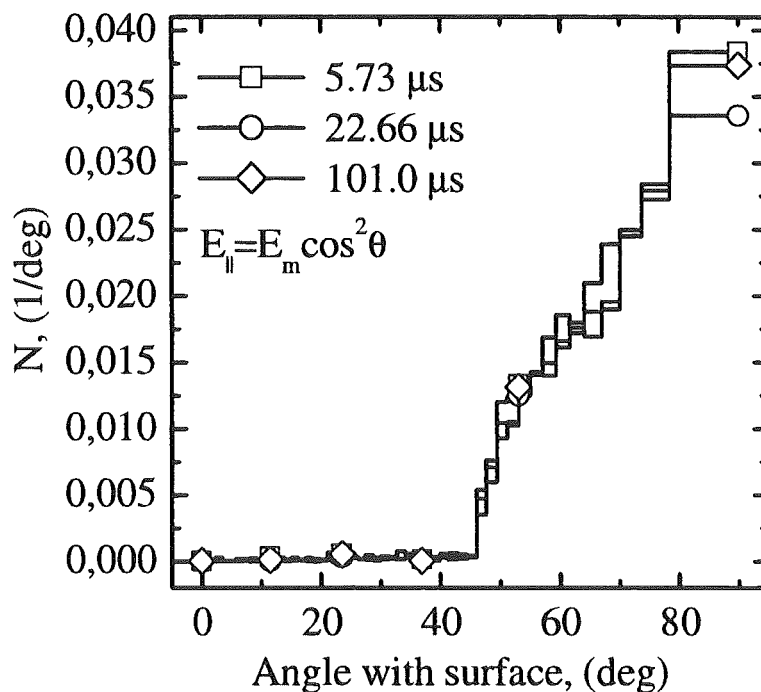


Fig. 52. Angular spectra of the Maxwellian distributed electrons with the longitudinal energy $E_{\parallel} = E_m \cos^2 \theta$ reflected from the inhomogeneous plasma shield. E_m - Maxwellian distributed energy of the incident electrons with temperature 10 keV, magnetic field $B = 5$ T, θ - isotropic pitch angle.

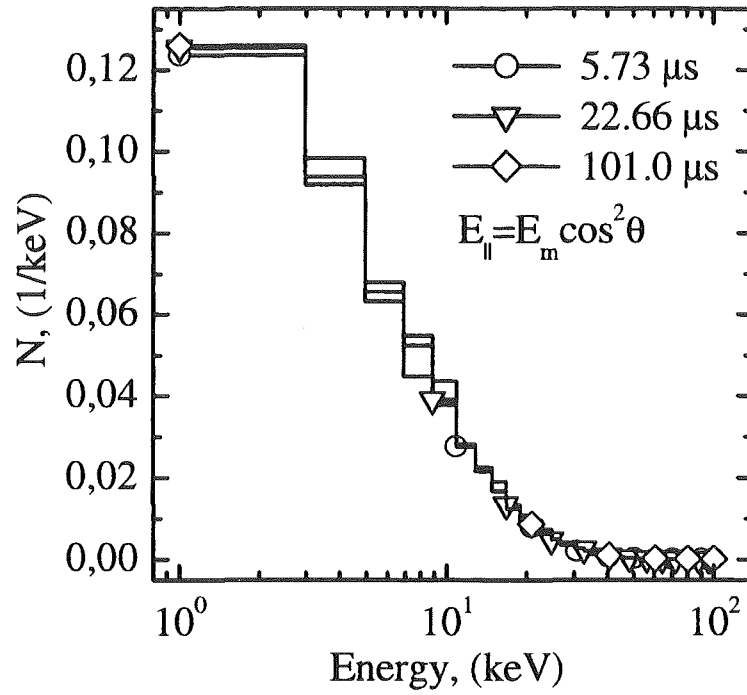


Fig. 53. Energy spectra of the Maxwellian distributed electrons with the longitudinal energy $E_{||} = E_m \cos^2 \theta$ reflected from the inhomogeneous plasma shield. E_m - Maxwellian distributed energy of the incident electrons with temperature 10 keV, magnetic field $B = 5$ T, θ - isotropic pitch angle.